Conservation of molecular responses upon viral infection in the non-vascular plant *Marchantia polymorpha*

Eric Moner-Ros[1*], Tamara Jiménez-Góngora[1*], Luis Villar-Martín[1], Lana Vogrinec[2,3], Víctor M. González-Miguel[4], Denis Kutnjak[2] and Ignacio Rubio-Somoza[1,5,]

[1]Molecular Reprogramming and Evolution (MoRE) Laboratory, Centre for Research in Agricultural Genomics (CRAG), CSIC-IRTA-UAB-UB, Campus UAB-Edifci CRAG. 08193 Cerdanyola del Vallés, Spain.

[2]National Institute of Biology, Department of Biotechnology and Systems Biology, Ljubljana, Slovenia.

[3]Jožef Stefan International Postgraduate School, Ljubljana, Slovenia.

[4]Data Analysis area, Bioinformatics Core Unit, Centre for Research in Agricultural Genomics (CRAG), CSIC-IRTA-UAB-UB, Campus UAB-Edifci CRAG. 08193 Cerdanyola del Vallés, Spain.

[5]Consejo Superior de Investigaciones Científicas (CSIC), Barcelona 08001, Spain.

*Those authors contributed equally to this work

To whom correspondence should be addressed: Ignacio.rubio@cragenomica.es

Abstract

After their transition from water to land around 450 million years ago, plants colonized new habitats facing unprecedented pathogenic microbes. After their first arrival to land, their further expansion reaching new habitats was mostly supported by a growing anatomical complexity in plants based on the acquisition of developmental innovations, such as roots, stomata and vascular tissue. Despite several of those innovations became central for the interaction between plants and their associated microbes, little is known about their impact on plant immune programs and on the diversification of infection strategies of their pathogens. A paradigmatic case is the close relationship between plant vasculature and viruses. Vascular tissues provide a unique cellular environment for viral replication and existence, besides constituting a fast track for viral systemic spread throughout the plant. Since most of our knowledge about plant-virus interactions come from studies in vascular plants, we here present a comparative study to contribute to the understanding of the evolution of plant-virus interactions by molecularly characterizing the interplay between the bryophyte *Marchantia polymorpha* and viruses. Virome analysis of Marchantia plants shows that they are primarily associated with RNA viruses in

natural settings. Additional molecular characterization of the interaction between Marchantia and tobacco mosaic virus (TMV) show conserved basic processes with vascular plants and divergent features. Viral infection triggers an extensive transcriptional reprogramming in Marchantia encompassing broad range defense responses, inhibition of cell cycle and photosynthesis and a sustained wound response that prevents further viral movement. Additionally, infected plants show premature aging and organ maturation. Notably, we found that some core responses that occur in infected areas in Marchantia, were described to be restricted to vascular tissues in Nicotiana, suggesting that evolutionary appearance of developmental innovations that became central in plants-virus interactions resulted in re-routing of defense responses. Finally, we uncover the conserved role of a transcription factor interacting with the TMV silencing suppressor p126 in specifically abrogating TMV infection.

Introduction

It is estimated that plants developed a functional vascular system through repurposing of pre-existing genes around 420 million years ago, which facilitated the growth of larger plants by providing mechanical support and enabling long distant transport of water, nutrients, and signalling molecules (Bowles et al., 2022, Lucas et al., 2013). Viruses are obligate parasites that can infect virtually any living organism hijacking central host cellular functions to replicate and spread within and intra hosts. Coincidentally with land colonization, the repertoire of viruses (virome) associated to plants enlarged and diversified both in nature and infection strategies. Although our current knowledge lacks information about virome composition at intermediately divergent plant lineages, it appears that viruses with large DNA genomes majorly infecting unicellular chlorophyte algae were displaced by an increasing population of viruses with RNA and small DNA genomes found in vascular plants (Mushegian et al., 2016). Plant vasculature has become central for the success of viral infections in tracheophytes, not only serving as fast track for viral systemic spread, but also providing a unique cellular environment for some viruses which replication is restricted to that tissue (Kappagantu et al., 2020). Accordingly, vascular cells are thought to present specific responses to viral infection when compared to other leaf cell-types (Collum and Culver, 2017).

Our current understanding of the molecular events governing plant-virus interactions is vastly shaped by studies focusing on vascular plants, mainly crops. Plants respond to viral infections via

63 at least three different but interconnected defense mechanisms (Mandadi and Scholthof, 2013).
64 Firstly, plants have an extracellular surveillance system that monitors the presence of pathogens
65 through the recognition of highly conserved microbe patterns dubbed as Pattern-associated
66 molecular patterns (PAMPs), such as viral derived double-strand RNAs (dsRNAS), the bacterial
67 flagellin or the fungal chitin. Detection of those molecules by specialized surface-localized
68 receptor kinases (Pattern recognition receptors, PRRs), triggers a first layer of defense called
69 PAMP-triggered immunity (PTI). PRRs expression is often restricted to focal points for microbial
70 interaction and invasion (Beck et al., 2014, Yotsui et al., 2023). Two additional surveillance
71 mechanisms monitor the intracellular presence of microbe-derived molecules. Highly stable
72 dsRNAs produced by viruses during their life cycle, independently of the DNA or RNA nature of
73 their genomes, are detected by the RNA silencing machinery which constitutes a conserved
74 antiviral defense mechanism both in plants and animals (Ding et al., 2018, Ding and Voinnet,
75 2007). Additionally, RNA silencing machinery also recognizes dsRNA generated from the
76 conversion of exogenous and endogenous single strand RNAs (ssRNA) by RNA-dependent RNA
77 polymerases (RDRs). RDR1 and RDR6 have been involved in antiviral defense in *Arabidopsis*
78 *thaliana* and *Nicotiana tabacum* (Garcia-Ruiz et al., 2010, Rakhshandehroo et al., 2017, Ying et
79 al., 2010), even though *Nicotiana benthamiana* has only a functional RDR6 (Bally et al., 2015).
80 Upon recognition, viral dsRNAs are trimmed in small RNAs (visRNAs) of 21 to 24 nucleotides in
81 length by members of the DICER-like family, mainly DCL2, DCL3 and DCL4 in Arabidopsis and
82 Nicotiana (Garcia-Ruiz et al., 2010, Lewsey and Carr, 2009). The resulting visRNA duplexes are
83 subsequently loaded into proteins from the ARGONAUTE family, which are the core elements of
84 the RNA-induced silencing complex (RiSC), and used to scan the intracellular space for the source
85 of dsRNA precursors in a sequence complementary manner abrogating viral infection (Lopez-
86 Gomollon and Baulcombe, 2022). In turn, viruses produce countermeasures, known as silencing
87 suppressors, targeted to interfere with different steps of the host RNA silencing machinery
88 (Lopez-Gomollon and Baulcombe, 2022). In response to these silencing suppressors, host micro
89 RNAs (miRNA, one of the two main classes of endogenous sRNAs in plants) are no longer
90 functional, allowing the translation of their targets and licensing a new layer of defense. Among
91 the miRNA targets involved in such counter-counter measure, members of the Nucleotide-
92 binding domain leucine-rich repeat (NLR) family are central. Thus, it has been suggested that
93 host miRNAs might work as sensors for the presence of pathogen-derived silencing suppressors
94 enabling a rapid host defense response based on the activation of otherwise silenced miRNA
95 targets (Vasseur et al., 2022, Silvestri et al., 2024). NLRs are core elements of the third

96 intracellular surveillance system for directly monitoring the intracellular presence of pathogen-
97 derived molecules, such as the prototypical case of the tobacco mosaic virus (TMV) replicase by
98 the gene *N* in tobacco (Erickson et al., 1999), or their impact on host cellular homeostasis. NLR-
99 activation triggers the so-called Effector-triggered immunity (ETI), which normally triggers a
100 hypersensitive response (HR) culminating in cell death. Those three defense systems, PTI, RNA
101 silencing and ETI largely rely on the action of the plant hormone Salicylic acid (SA). PTI and ETI
102 responses encompass activation of SA signalling (Pruitt et al., 2021) while SA activates RDR1 in
103 Arabidopsis and Nicotiana (Lee et al., 2016, Ying et al., 2010, Yu et al., 2003). Additionally, RDR1
104 expression is also induced by treatment with jasmonates (Liu et al., 2009, Xu et al., 2013),
105 another central hormone in plant defense. Many of those immunity components and networks
106 were already present in the last common land plant ancestor, while others have been acquired
107 alongside the increasing plant cellular and anatomical complexity (de Vries et al., 2018, Belanger
108 et al., 2023, Chia et al., 2024).

109 A Central question in plant-microbe interactions is how the evolution of different plant
110 developmental trajectories, including the acquisition of major innovations, impacts host defense
111 and pathogen infection strategies. In animals, comparative studies have proved very informative
112 about the origin and diversification of their innate immune responses against virus (Iwama and
113 Moran, 2023). Likewise, comparative studies including non-vascular plants, like the liverwort
114 *Marchantia polymorpha*, have been instrumental in understanding the evolution of the
115 interactions between plants and pathogens other than viruses (Carella et al., 2018, Gimenez-
116 Ibanez et al., 2019, Redkar et al., 2022). Comparative studies in plants have traditionally relied
117 on both model plant species and microbes, despite the lack of prior experimental evidence that
118 those interactions occur in nature. Incorporating bryophytes into those comparative studies not
119 only provides important information about how plant immune programs may have evolved, but
120 it also bears the potential to determine the contribution of developmental innovations, such as
121 roots, stomata or vasculature, to their diversification.

122 To enable comparative studies towards understanding the evolution of plant-virus interactions,
123 we here present the characterization of the molecular interplay between the non-vascular
124 liverwort *Marchantia polymorpha* and viruses. We firstly defined the composition of the virome
125 of Marchantia plants living in the wild and used that information to select a virus with similar
126 genomic features to those found in nature for further molecular characterization and that can
127 be tagged with a fluorescent protein that enables monitoring of infection. Additionally, the

128 selected virus should be able to infect a broad range of hosts, in which their molecular
129 interactions have been studied. Following those criteria, we focused on the first ever isolated
130 virus, the tobacco mosaic virus (TMV). TMV is a ssRNA virus from the Tobamovirus genus
131 showing a broad host range in nature (Zamfir et al., 2023). Additionally, TMV has been
132 extensively used for studying plant-virus interactions in a wealth of plant species, including
133 several Solanaceae species, like tomato and tobacco, and the model plant *Arabidopsis thaliana*,
134 which provide strong foundation for comparative studies. TMV infects through wound entry
135 points from where it moves cell-to-cell via plasmodesmata, until it reaches the vascular system
136 for systemic infection of distal parts of the plant following the stream of photoassimilates (Liu
137 and Nelson, 2013).

138 Our results show that *Marchantia polymorpha* is associated with RNA viruses in natural
139 populations that can replicate in lab grown Marchantia plants. Additionally, TMV can replicate in
140 Marchantia plants triggering a conserved transcriptional reprogramming encompassing
141 increased wounding and PTI responses in detriment of photosynthesis and cell cycle progression
142 and leading to changes in life-history traits, such as aging and senescence. Induction of a wealth
143 of NLR proteins and core elements from the RNA silencing machinery were also observed,
144 including DCL4 that, in absence of a DCL2 gene in the Marchantia genome (Belanger et al., 2023),
145 seems to be the main antiviral DCL protein according to the predominant 21 nuleotides in length
146 presented by TMV-derived vsRNAs. Noteworthy, the general response of the RNA silencing
147 machinery observed in Marchantia upon TMV infection is equivalent to that found specifically in
148 vascular tissues of *Nicotiana benthamiana*, suggesting an evolutionary anatomical rerouting of
149 antiviral defense towards newly acquired focal points for viral infection.

150 We additionally identified a conserved host interactor with the TMV silencing suppressor p126
151 that triggers cross-species defense against TMV.

152 **Results**

153 ***Marchantia polymorpha* is associated to RNA viruses in nature.**

154 To identify viruses associated with *Marchantia polymorpha* in nature, we performed a
155 virome analysis of two composite plant samples including 21 individuals growing naturally, not
156 cultivated, in 5 different locations spanning 4 different countries and accessible to possible viral
157 vectors. First contained Marchantia individuals obtained from three open air botanical gardens
158 throughout Europe: Tübingen (Germany), Bern (Switzerland) and Cambridge (UK). The second

159 encompassed individuals growing open air at the botanical garden in Osnabrück (Germany) and
160 individuals growing in urban sites in Ljubljana (Slovenia). In addition to the expected background
161 of bacteriophage sequences, we detected several known viruses, including some capable of
162 infecting or being associated with plants, fungi or invertebrates (Supplementary Table 1).
163 Putatively new virus-like sequences, possibly associated with *M. polymorpha*, were selected for
164 further analyses from the first dataset, based on i) their relatively high average sequencing
165 depths and ii) similarity to viruses previously associated with eukaryotic organisms, including
166 plants and invertebrates (Supplementary Table 2). Two previously described and three newly
167 identified viruses were hence selected for further RT-qPCR confirmation of their association with
168 the different *M. polymorpha* individuals, along with plants from the Tak-1 reference accession
169 grown in sterile conditions. Specific primers to detect Ligustrum necrotic ringspot virus (LNRV,
170 known to infect plants), Hubei picorna-like virus 51, (detected in a metagenomics study and
171 putatively associated with diverse sample types by datamining – see results below) a newly
172 identified picorna-like virus (which we named Tübingen picorna-like virus 1, with average
173 mapping depth of 2230x and contig length of 7801 nts), a new tombus-like virus (Tübingen
174 tombus-like virus 1, with average mapping depth of 218x and contig length of 4521 nts), and a
175 new sobemo-like virus (Bern sobemo-like virus 1, with average mapping depth of 88x and contig
176 length of 2569 nts) were used for these analysis. While none of those viruses were detected in
177 negative control Tak-1 plants, individuals from Tübingen were associated with all tested viruses
178 but the Bern sobemo-like virus 1, which in turn was present in individuals from Bern along with
179 Tübingen picorna-like virus 1. Individuals from the Cambridge population were associated with
180 Hubei picorna-like virus 51 and Tübingen picorna-like virus 1 (Supplementary Table 3). Further,
181 we used a datamining approach to search for the presence of conserved RdRp domain
182 fingerprints (palmprints) of the selected viruses in global short reads sequence datasets using
183 Serratus infrastructure (Edgar et al., 2022). The results of the analysis suggested that palmprint
184 RdRp sequences with high similarity to those of queried viruses, can be associated with diverse
185 sample types, mostly including environmental samples, such as wastewater, water, rhizosphere,
186 soil and plants (Supplementary Table 4).

187 Given that Tübingen picorna-like virus 1 was present in all tested populations from the first
188 sampling, we decided to further characterize its genomic features and interaction with
189 *Marchantia polymorpha*. Indeed, Tübingen picorna-like virus 1 had the highest mapping depth
190 of all contigs in our virome analysis and showed a similar genome structure as other unclassified

191 picorna-like viruses (Shi et al., 2016), consisting of two predicted genome open reading frames
192 (ORFs), first containing domains with homology to superfamily 3 helicase, peptidase C3 and RNA-
193 dependent RNA polymerase (RdRp) and second three domains with homology to a coat protein
194 with 8-stranded jelly roll β-barrel motif (Figure 1A). Phylogenetic analysis (Figure 1B) of the RdRp
195 protein sequence and its closest NCBI GenBank homologues showed high similarity (80% identity
196 of aligned sequences) of this virus isolate with a recently reported plant associated picorna-like
197 virus (Trichosanthes kirilowii picorna-like virus, QKK82970.1). Much lower identities were
198 observed for Tübingen picorna-like virus 1 (29-42%) and other viruses associated with diverse
199 sources (plants, gastropods, water, crayfish, artropods and bird feces). However, given that they
200 were discovered in metagenomics studies their association with these hosts is only speculative.
201 Thus, we performed and additional phylogenetic analysis, comparing the RdRp sequence of
202 Tübingen picorna-like virus 1 with most similar RdRp sequences from RNA Viruses in
203 Metatranscriptomes (RVMT) database (https://riboviria.org/) (Neri et al., 2022). The analysis
204 revealed high similarity of the viral RdRp to several sequences included in family-level cluster
205 f.0032 with order *Picornavirales* (Supplementary Figure 1A). Even if this cluster contains diverse
206 representatives, none of those has confirmed host associations at the moment (Supplementary
207 Table 5). Similarly, as found in Serratus analysis, sequences most similar to investigated virus
208 were associated, e.g., with wastewater, wetlands, and peat soil samples (Supplementary figure
209 1b, Supplementary Table 5).

210 Next, we tested whether the Tübingen picorna-like virus 1 was able to replicate in *M. polymorpha*
211 by incubating two-weeks old Tak-1 individuals with extracts isolated from the Tübingen
212 population, which contained the highest levels of Tübingen picorna-like virus 1, as determined
213 by RT-qPCR analysis, or from Tak-1 plants grown in sterile conditions. Individual Marchantia
214 plants were collected one and two weeks after incubation and the levels of viral accumulation
215 were measured by RT-qPCR. Individuals exposed to extracts from virus-positive plants showed a
216 trend of increased viral levels over time, while no amplification was observed in plants incubated
217 with extracts from Tak-1 plants (Figure 1C). This indicated that Tübingen picorna-like virus 1 can
218 replicate in Marchantia.

219 Collectively, those results show that *Marchantia polymorpha* can be associated with RNA viruses
220 in nature.

221 Additionally, we performed data mining to search for possible DNA viruses associated with
222 *Marchantia polymorpha*. Sequencing data from 74 biological samples (obtained from natural

223 environments; Beauliue et al., 2023) was analyzed for the presence of viral contigs. Analysis
224 revealed that most of the examined samples contained virus-like sequences, with the majority
225 exhibiting similarity to bacteriophages (Supplementary Table 6). Within the dataset we also
226 found virus-like sequences with similarity to members of *Phycodnaviridae,* which can infect
227 unicellular green algae. Since only few relatively short contig sequences like this group of viruses
228 were identified in different datasets, and the data was primarily not produced with microbiome
229 study in mind (e.g., no surface washing) the association with *M. polymorpha* with viruses from
230 this taxon is dubious and could be further explored in future studies.

231 **Tobacco mosaic virus replicates in *Marchantia polymorpha***

232 Since its identification in the 19th century, tobacco mosaic virus has been extensively used for
233 studying plant-virus interactions in several vascular plant species like Arabidopsis and Nicotiana
234 (Scholthof, 2004). As a first step for comparative studies on plant-virus interactions between
235 vascular and non-vascular plants, we aimed to infect *Marchantia polymorpha* plants with a GFP
236 labelled clone of TMV (Peart et al., 2002). Sap from leaves of healthy and infected *Nicotiana*
237 *benthamiana* plants were isolated and used to incubate two-weeks old Tak-1 plants grown in
238 sterile conditions. After incubation, Marchantia plants were transferred to soil and part of the
239 remaining sap was inoculated mechanically with an abrasive (carborundrum) in basal leaves
240 from 1 month old Nicotiana plants, as control for its infectivity. After two weeks, Nicotiana plants
241 showed systemic GFP signal under UV light along with symptoms of infection (Supplementary
242 Figure 2), whereas Tak-1 plants displayed GFP signal in discrete infection foci that increased their
243 size over time (Figure 2A, Supplementary Figure 3), suggestive of viral replication. This was
244 further corroborated by RT-qPCR amplification of pooled samples including four GFP positive
245 individuals at the first (T1) and second weeks after incubation (T2), in comparison with mock and
246 freshly incubated (T0) plants (Figure 2B, Supplementary Figure 4). sRNA profiling in GFP positive
247 areas from Marchantia thalli identified TMV-derived vsRNAs enriched in 21 nucleotides long
248 fragments, consistent with DCL4-mediated processing, and mapping to the TMV-GFP sequence
249 (Figure 2C, Supplementary Figure 5).

250 Histological sections of the infected area showed presence of the virus in all cell types, as inferred
251 from GFP fluorescence and when compared to sections from mock treated plants, suggesting no
252 preference for a specific cell-type during viral infection (Figure 2D).

253 Those results confirmed that TMV can replicate in *M. polymoprha* plants pointing to Marchantia-
254 TMV as a suitable pathosystem for comparative studies.

255 **TMV infection triggers profound molecular reprogramming in *M. polymoprha***

256 To characterize the molecular reprogramming caused by TMV infection, we performed
257 transcriptomic assays. TMV-GFP infected tissue was collected in four pools including 5 plants
258 each, along with the very same area from mock treated plants as control (Supplementary Figure
259 6A). RNA was isolated and the presence of TMV was confirmed by RT-qPCR in each pool
260 (Supplementary Figure 6B). Principal component analysis (PCA, Supplementary Figure 6C) of the
261 transcriptome supported the RT-qPCR results showing a clear separation of infected and mock
262 samples. Since separation among infected samples correlated with viral RT-qPCR levels, we
263 selected the three replicates that had the highest levels of TMV and clustered together for
264 further analysis. A total of 1879 genes were found to be up regulated while 1645 were reduced
265 (padjust<0.05, Log2(fold-change) =1) in response to TMV infection (Supplementary Table 7).
266 Consistently with an ongoing pathogenic interaction, we found several defense related marker
267 genes among the differentially expressed genes (DEG). Members of the pathogenesis-related
268 (PR) family are prime markers of immune responses in several plant species, including
269 Marchantia (Carella et al., 2019, Gimenez-Ibanez et al., 2019) and we found that the expression
270 of several homologues showed opposite expression patterns when compared to mock treated
271 plants (Supplementary Table 8). Several PTI marker genes have been identified in Marchantia
272 based on their orthology to those established in Arabidopsis (Gimenez-Ibanez et al., 2019) and
273 their activation in the presence of bacterial and fungal extracts (Gimenez-Ibanez et al., 2019,
274 Redkar et al., 2022). We observed that a set of those conserved PTI markers were also induced
275 in response to TMV infection (Figure 3A). Additionally, a significant number of intracellular
276 receptors from the NLR family displayed upregulated expression upon TMV infection ($p < 6.245e-$
277 05 with those described by (Bowman et al., 2017); $p < 1.308e-05$ with those described by (Chia
278 et al., 2022, Chia et al., 2024); Supplementary Table 9). Nevertheless, in line with the absence of
279 TNL genes in Marchantia (Chia et al., 2024), none of those showed significant sequence similarity
280 to the NLR N gene triggering ETI responses in TMV infected tobacco plants (Whitham et al.,
281 1994). Likewise, several components from the RNA silencing machinery upregulated in tobacco
282 plants upon TMV infection (Sheng et al., 2019), were also differentially expressed in response to
283 TMV in Marchantia plants. The non-canonical MpDCL1b (Mp6g09830), MpDCL4 (Mp7g11720),

284 and MpRDR6 (Mp8g14970) were upregulated, whereas MpDCL3 (Mp1g02840), MpAGO9
285 (Mp8g08610) and MpNRPE1b (Mp6g00230) were suppressed.

286 Gene Ontology (GO) analysis of the upregulated genes revealed an enrichment (padjust<0.05)
287 of biological processes related to reactive oxygen species, wounding, light intensity, heat
288 responses and responses to fungus and the presence of their constituent chitin (Supplementary
289 Table 10, Supplementary Figure 7A). Photosynthesis, DNA packaging and cell cycle, microtubule
290 organization or regulation of salicylic acid metabolism were among the downregulated processes
291 (padjust<0.05; Supplementary Table 11, Supplementary Figure 7B).

292 Notably, TMV is mainly transmitted through wounds and wounding response was one of the
293 processes to which upregulated genes belonged in the GO analysis, which prompted us analysing
294 this response. ERF transcription factors are central to trigger wounding responses in vascular
295 plants such as *A. thaliana* (Heyman et al., 2018) with a conserved set of ERF transcription factors
296 being also recently described to respond to wounding in *Marchantia polymorpha* plants (Liang
297 et al., 2022). A subset of these wounding responsive ERF transcription factors showed the same
298 expression pattern upon TMV infection as that observed upon intensive wounding (Figure 3B,
299 (Liang et al., 2022). To determine the whole transcriptional overlap between wounding and TMV
300 responses, we reanalysed published tissue incision transcriptomic responses (Liang et al., 2022)
301 using the same pipeline we used for the TMV samples. Comparison of both datasets showed a
302 significant overlap both in up-regulated (593 genes; p<6.631e-235) and down-regulated genes
303 (162 genes; p<2.137e-70; Figure 3C), suggesting that TMV infection contributes to a sustained
304 wound response in Marchantia.

305 Chitin is one of the most abundant polysaccharides in nature and it is a primary component of
306 cell walls in fungi and exoskeletons of arthropods such as insects, which in turn can work as viral
307 vectors in a range of plants species (Campbell, 1996). According to the GO enrichment in
308 response to chitin and fungi, and besides the fungal responsive genes described above as part
309 of a conserved PTI response, we also observed upregulation of a set of fungal responsive WRKY
310 transcription factors (Figure 3D; (Redkar et al., 2022, Yotsui et al., 2023).

311 Photosynthetic deficiency is a hallmark for several stress responses, including those involving
312 viral infections. Accordingly, downregulation of transcripts involved in photosynthesis was one
313 of the main processes affected in our GO study as consequence of TMV infection. We determined
314 the photosynthetic efficiency in TMV infected areas from 10 4-weeks old Tak-1 plants after 2-

315 weeks of infection along with the very same area in mock treated plants. TMV infected areas
316 showed a significant reduction in photosynthetic competency when compared to similar areas
317 from mock treated plants (Figure 3E). Notably, parts of those very same plants distant to the
318 infection foci, showed also reduced photosynthetic capability, although to a lesser extent (Figure
319 3F). Those results suggest that TMV responses might be systemic in *Marchantia polymorpha*
320 plants.

321 Overall, those results show that TMV engages in a compatible interaction with *Marchantia*
322 *polymorpha*.

323 **Salicylic and OPDA-dependent signaling pathways are active at TMV infected areas.**

324 The plant hormones Salicylic acid (SA) and Jasmonic acid (JA) are central in defense responses
325 against most pathogens of vascular plants, acting both in a synergistic and antagonistic manner.
326 Whereas the SA biosynthesis and signalling pathway are mostly conserved in *Marchantia*
327 *polymoprha* (Jia et al., 2023), the active molecules binding to the COI1 receptor and triggering
328 jasmonate signaling are a group of long chain polyunsaturated fatty acids, including dinor-OPDA,
329 instead of JA-Ile (Kneeshaw et al., 2022, Monte et al., 2018). Therefore, we compared the SA and
330 jasmonate-related transcriptomic responses with those found during TMV infection. To that end,
331 we used the time course datasets obtained on incubation of Marchantia with 1mM SA during 2,
332 6 and 12 hours (Jeon et al., 2022), SA concentration shown to promote defense against bacterial
333 and to increase susceptibility to fungal pathogens (Jeon et al., 2022, Matsui et al., 2020).
334 Comparison of the DEGs identified on SA treatment showed a significant overlap with those
335 responding to TMV infection (Figure 4A; Supplementary Figure 8). A total of 225 genes were
336 commonly up-regulated by 2 hours SA treatment or TMV ($p<1.799e-100$), 306 ($p < 1.382e-172$)
337 were shared after 6 hours treatment, and 92 ($p < 3.580e-47$) by 12 hours of SA incubation.
338 Likewise, TMV infection shared 47 down regulated genes ($p<1.618e-14$) with 2 hours, 38 ($p <$
339 $2.897e-13$) with the 6 hours, and 17 genes with 12 hours incubation samples ($p < 1.720e-05$),
340 showing that TMV infection activates SA-dependent transcriptional responses.

341 To ascertain a possible contribution from the jasmonate signalling pathway, we compared the
342 TMV transcriptional response with that of plants treated with dn-OPDA (Monte et al., 2018) or
343 having a constitutively activated jasmonate pathway as a consequence of the mutation of the
344 JAZ signalling repressor (Mpjaz-1 KO plants; (Monte et al., 2019). A total of 143 and 81 genes
345 were commonly up-regulated upon TMV infection and *Mpjaz* deficiency or dn-OPDA treatment,

346 while 238 were downregulated in TMV infected and Mpjaz-1 KO plants (Figure 4B), suggesting
347 that TMV infection also activates the jasmonate signalling pathway in Marchantia. Finally, we
348 found that 64 genes were commonly up-regulated by TMV infection, SA 6 h treatment and
349 absence of a functional MpJAZ protein, while 54 genes were up-regulated by TMV infection, SA
350 6h and dn-OPDA treatments (Figure 4C).

351 Next, we performed a GO analysis in the different sets of genes that were found to be commonly
352 regulated by TMV infections and each of the different hormone-related transcriptomes (i.e. Up
353 regulated genes by TMV and SA 6 h treatment from Figure 4A). That approach showed that the
354 JA pathway might contribute to the activation of wounding, reactive oxygen species and virus
355 responses, in addition to the catabolism of several compounds, including lipids,
356 phenylpropanoids and salicylic acid, in TMV infected Marchantia plants. Interestingly, some of
357 these processes were also commonly upregulated by TMV infection and SA treatment, including
358 wounding, SA and lignin catabolism among others. The SA response pathway might on the other
359 side also contribute to the observed transcriptional up-regulation of defense genes against
360 bacteria and fungi, as well as responsive to chitin in TMV infected plants (Figure 4D,
361 Supplementary Table 12). Amongst the downregulated processes by MpJAZ deficiency and TMV
362 infection were translational elongation, mucilage and cell wall biosynthesis, response to
363 fructose, photosynthesis, microtubule-based process, growth, and response to abscisic acid
364 (ABA; Figure 4E, Supplementary Table 12)

365 Furthermore, genes found to be commonly upregulated by TMV, SA and dn-OPDA treatment
366 were related to oxylipin and phenylalanine metabolism, wounding and drought recovery, among
367 other Gene ontology groups(Figure 4F; Supplementary Table 13). Meanwhile, those genes found
368 to be commonly upregulated by TMV infection, SA 6 h treatment and enhanced JA signalling in
369 Mpjaz-1 plants were related to antiviral defense and lipid catabolism, which has been also
370 recently found to contribute to SA activation and antiviral defense ((Xu et al., 2022); Figure 4G,
371 Supplementary Table 13)

372 Collectively, those results suggest that SA and JA signalling pathways are activated in Marchantia
373 during TMV infection.

374 **TMV infection triggers aging in *Marchantia polymorpha.***

375 Interactions with pathogens, including viruses, can result in the modification of life-history traits
376 and developmental trajectories both in plants and animal (Pagan et al., 2008, R.C., 1978).

377 Senescence is the final stage of the life cycle of a cell, tissue or organism and it is gradually
378 triggered throughout aging. This process can be accelerated by the interaction with different
379 pathogens, including the crucifer infecting TMV-Cg strain capable of compatible interactions with
380 the Arabidopsis UK-4 ecotype (Espinoza et al., 2007, Lim and Nam, 2005). Wound response,
381 mitotic cell arrest, and reduced photosynthetic efficiency are hallmarks for plant cell senescence
382 (Espinoza et al., 2007, Gan, 2003). Additionally, SA and JA, along with ET, contribute to
383 senescence in *Arabidopsis thaliana* (Schommer et al., 2008, Yu et al., 2021).. Since all those
384 senescence hallmarks were present in our molecular characterization of the Marchantia-TMV
385 interaction, we first checked the expression levels of several senescence marker genes in our
386 transcriptomic data (Kulshrestha et al., 2022). We found that many of those senescence markers,
387 such as MpMYB14 (Mp5g19050), MpORE1 (Mp2g07720), MpNYE1 (Mp1g17090) and MpWRKY7
388 (Mp3g17660), were induced upon TMV infection, hence suggesting that TMV infection could
389 trigger aging and tissue maturation in Marchantia. Transcriptional trajectories orchestrating
390 maturation and aging in Marchantia, both at organism and tissue level, have been recently
391 reported through transcriptional studies over developmental time, including individuals from
392 different ages (spanning from 1 day after germination - D1- to 31 days old Marchantia plants -
393 D31) , or by analysing sections along the thalli from top to base, being slice 1 (S1) at the top,
394 considered the youngest part of the organ, and being slice 6 (S6) at the base and considered the
395 oldest (Wang et al., 2023). To assay whether TMV infection could modified the life-history of
396 Marchantia plants we compared the transcriptional profile from mock and TMV infected
397 Marchantia plants with those from the maturation and developmental trajectories. Clustering
398 the transcriptional profile of mock and TMV infected plants with those datasets, based on
399 Pearson's correlation coefficient and regression model, showed that TMV infection promotes
400 maturation and aging. Thus, while the transcriptome from mock treated plants clustered with
401 juvenile state samples (slide 2 and Day 1), that from TMV infected plants clustered with slide 4
402 and day 31 of development (Figure 5A, 5B).

403 Those results indicated that TMV infection triggers premature tissue maturation and senescence
404 in Marchantia, a characteristic trait from compatible plant - virus interactions.

405 **MpNAC7 is a conserved interactor of the TMV silencing suppressor p126 and enhances defense**
406 **against TMV in tobacco plants.**

407 The TMV replicase p126 is essential for viral replication and movement, but it also works as a
408 silencing suppressor in vascular plants (Ding et al., 2004). To gain insights into its possible role

409 during TMV infection in Marchantia plants, we first established its subcellular localization. We
410 found that p126 fused to GFP accumulated within the cytoplasm and, occasionally, as discrete
411 spot-like inclusions (Figure 6A) consistently with earlier studies in onion epidermal cells, where
412 the full length p126 protein fused to GFP was found associated to the endoplasmic reticulum
413 (dos Reis Figueira et al., 2002).

414 Constitutive expression of viral-derived silencing suppressors often leads to plant developmental
415 defects, like growth stunting (Kasschau et al., 2003). Accordingly, four-weeks old Marchantia
416 plants constitutively expressing p126 were smaller in size when compared to control plants
417 (Figure 6B, Supplementary Figure 9).

418 The TMV replicase p126 is known to associate with several host factors in Arabidopsis, including
419 TOM1 (Yamanaka et al., 2000), GDI2 (Kramer et al., 2011) and the transcription factor ATAF2
420 (Wang et al., 2009). To assess whether those interactions were conserved between p126 and the
421 corresponding orthologs in Marchantia, we performed Y2H assays. Orthologs were identified by
422 blasting the Arabidopsis protein sequences at MarpolBase (https//Marchantia.info) and
423 PlantRegMap (http://plantregmap.gao-lab.org/). The P126 full length and helicase domain
424 (Δp126, nt 2442 to 3636) were fused to the GAL4 binding domain and used as baits, while the
425 putative interactors fused to the GAL4-activation domain, were used as preys. Notably, the only
426 conserved interaction was that of the ortholog of the NAC transcription factor ATAF2, *MpNAC7*
427 (Mp6g02620), with Δp126 (Figure 6C). As for Δp126-ATAF2 binding (Wang et al., 2009) Δp126-
428 MpNAC7 interaction could be confirmed *in planta* using bimolecular luminescence
429 complementation (Figure 6D). Additionally, both the helicase domain alone and the full-length
430 p126 were found to interact *in planta* with either NAC transcription factors. Such discrepancy
431 between the results obtained by the two different protein-protein assays can be potentially
432 attributed to the presence of additional protein partners in Nicotiana or variable intracellular
433 conditions, such as pH, that modify protein folding allowing the interaction with the full length
434 p126.

435 In Arabidopsis, ATAF2 expression is triggered by TMV infection (Wang et al., 2009). Likewise, we
436 found that MpNAC7 expression is also increased on TMV infection (Log2(fold-change)= 0.991),
437 wounding (Log2(fold-change)= 2.67), dn-OPDA and after 6 hours of SA treatment (Log2(fold-
438 change)= 1,23) in Marchantia. Likewise, ATAF2 is induced by wounding, SA and JA treatments
439 (Delessert et al., 2005) and contributes to defense against TMV in Arabidopsis (Wang et al.,
440 2009). Here, to ascertain the role of MpNAC7 in defense against TMV, and rule out a possible

441 connection with RNA silencing- mediated responses, we infected 1 month old Nicotiana plants
442 deficient in RDR6 (rdr6i; (Schwach et al., 2005)) with MpNAC7, or GUS as control, in the presence
443 of TMV or an unrelated ssRNA virus, such as turnip mosaic virus (TuMV). TMV and TuMV strains
444 were labelled with the ROS1 gene which triggers anthocyanin production, and hence we
445 followed presence of the viruses by the purple colour (Bedoya et al., 2012). We observed that
446 co-expression of MpNAC7 abrogated local and systemic TMV infection with respect to plants co-
447 expressing the GUS control. By contrast, MpNAC7 co-expression was of no effect on TuMV
448 infected plants, that displayed a similar local and systemic presence of the virus as the GUS co-
449 infiltrated controls (Figure 6E, Supplementary Figure 10).

450 Collectively, those results show that molecular interaction between the TMV silencing
451 suppressor p126 and the host NAC transcription factor is conserved in Marchantia, as well as the
452 role of this transcription factor in defense.

453 **Discussion**

454 In this work, we have characterized the interaction of the non-vascular liverwort *Marchantia*
455 *polymorpha* with viruses. First, we have defined known and unknown viruses that associate with
456 Marchantia in natural settings. These studies show that Marchantia is primarily associated with
457 RNA viruses in nature, validating previous predictions based on the presence of viral gene
458 hallmarks in the transcriptomes from the 1000 Plants Genome Project (Mushegian et al., 2016).
459 We also showed that at least one of these newly discovered viruses (Tübingen picorna-like virus
460 1) can replicate in laboratory grown Marchantia Tak-1 plants. In-depth phylogenetic analyses
461 placed this virus within a larger, poorly characterised cluster composed of viruses discovered
462 with metagenomics approaches, mostly associated with environmental samples, within
463 *Picornavirales* order. Viruses from this order infect mostly animals, but also protists and plants
464 (Koonin et al., 2020) Tübingen picorna-like virus 1 codes for the hallmark protein domains
465 characteristic for picornaviruses, but seems to lack movement protein (MP) that is present in
466 most of the plant-infecting viruses, with the exception of some vertically transmitted viruses,
467 e.g., from families *Paritiviridae* and *Amalgavirida (Dolja et al., 2020)*.Although kinetics of viral
468 replication is not linear, in our infection experiment we observed only modest virus titre increase
469 over time, which might be connected to limited ability of virus to move from cell-to-cell due to
470 the lack of MP. Few viruses have been identified by metagenomic approaches in non-vascular
471 plants, such as *M. polymorpha*, some with (Debat et al., 2023, Mifsud et al., 2022) and other
472 without MP (Mushegian et al., 2016, Vendrell-Mir et al., 2021). On the other hand, it is predicted

473 that plasmodesmata have evolved along with the acquisition of vasculature to assist in the
474 transport of nutrients throughout the plant by likely changing the way they control their aperture
475 (Benitez et al., 2018, Hernandez-Hernandez et al., 2020). Therefore, it is plausible that the way
476 in which viruses interact with host plasmodesmata to move from cell-to-cell has also differed
477 over time. Additionally, it has also been recently proposed that viruses lacking a MP can
478 systemically infect vascular plants exploiting host proteins that are also predicted to be present
479 in Marchantia, such as those belonging to the Phloem Protein 2 (PP2) gene family (Ying et al.,
480 2024). Since we only started to uncover *M. polymorpha* virome, and, at the same time, little is
481 known about the structure and function of *M. polymorpha* plasmodesmata (Zeinsmaster D.D
482 and Carothers Z.B, 1974), which are involved in interaction with MP in vascular plants, further
483 research on the topic, building also on *M. polymorpha* inoculation procedures developed in this
484 study, can shed a light on repertoire of viruses infecting non-vascular plants. Recent study
485 proposed a horizontal transfer of MP-encoding viruses infecting higher plants to nonvascular
486 plants (Butkovic et al., 2023), whereas discovery of Tübingen picorna-like virus 1 suggests
487 another possible route of virus emergence in non-vascular plants. This may be linked with
488 horizontal virus transfer from invertebrates or protists and could, very speculatively, represent a
489 missing link in a recently suggested evolution of single jelly roll type CP to MP (Butkovic et al.,
490 2023).

491 Second, we have found that TMV engages into a compatible interaction with Marchantia plants.
492 That interaction encompasses an extensive transcriptional reprogramming reminiscent of that
493 found in vascular plants such as Arabidopsis and Nicotiana, albeit involving also previously
494 uncovered differences like the activation of a sustained wounding response. Third, we have
495 found that the TMV silencing suppressor p126 displays similar subcellular localization in
496 Marchantia cells, as in onion epidermal cells (dos Reis Figueira et al., 2002), and that it interacts
497 with a NAC transcription factor ortholog of the Arabidopsis ATAF2 transcription factor involved
498 in defense against TMV (Wang et al., 2009), MpNAC7. Additionally, transient expression of
499 MpNAC7 specifically abrogates TMV infection in Nicotiana plants. All those commonalities show
500 that core molecular events of plant-virus interactions found in vascular plants might be also
501 present in non-vascular plants.

502 Marchantia plants infected with TMV undergo a transcriptional reprogramming consistent with
503 a pathogenic process and characterized by the activation of the defense related PR proteins and
504 a conserved PTI response. Perception of dsRNAs have been found to trigger PTI in response to

505 TMV infection in Arabidopsis, which in turn contributes to antiviral defense (Korner et al., 2013).
506 Indeed, dsRNA-triggered PTI is dependent on the Arabidopsis PRR co-receptor SERK1 (Niehl et
507 al., 2016), which has a corresponding ortholog in the Marchantia genome (Mp7g09160), and
508 which was shown to be involved in PTI against *Pseudomonas syringae,* and to be targeted by the
509 PTI suppressors AvrPto (Gimenez-Ibanez et al., 2019). Thus, it will be interesting in future studies
510 to analyse the role of MpSERK1 in viral PTI responses. Additionally, TMV infection triggers the
511 expression of a significant number of NLR genes that can potentially contribute to an ETI
512 response. While in *Nicotiana benthamiana*, both DCL2 and DCL4 process TMV RNAs into 22 and
513 21 nucleotides long vsRNAs (Guo and Wong, 2017), the solely presence of DCL4 in Marchantia
514 results in the predominant processing in 21 nucleotides long vsRNAs. We also observed changes
515 on the expression of core genes of the RNA silencing machinery in response to TMV infection. In
516 contrast to the repression of elements from the RNA-Directed DNA methylation pathway, such
517 as MpDCL3, MpAGO9 and MpNRPE1b, the central elements within the RNA antiviral machinery
518 MpDCL4 and MpRDR6 were activated. Such general switch on RNA silencing pathways in
519 Marchantia is reminiscent of that found specifically restricted to the vasculature of *Nicotiana*
520 *benthamiana* in response to TMV (Collum and Culver, 2017). Those results suggest an
521 evolutionary re-routing of defense mechanisms after acquisition of novel tissues or cell-types
522 that become new focal points for plant-virus interactions.

523 Interestingly, our results also uncover a previously unknown potential role of wound response
524 as an antiviral defense mechanism. Plant cells undergoing wound responses experience
525 inhibition of their photosynthetic ability becoming sink tissues on the transport of
526 photoassimilates (Quilliam et al., 2006), attracting TMV movement (Brants, 1961). This wound
527 response might be, at least partially, sustained by the activation of the salicylic and jasmonate
528 pathways. Thus, it is tempting to speculate that sustained wound response in Marchantia plants,
529 along with local and systemic decreased on photosynthetic capability, confine TMV infection
530 limiting its movement throughout the plant. Additionally, premature senescence of infected
531 tissues might further abrogate viral infection. Therefore, modification of host´s life-history traits,
532 such as senescence, can constitute a defensive mechanism in Marchantia.

533 Salicylic and jasmonate pathways are central for defense against several pathogens. Although
534 the interaction between both hormones has been traditionally considered antagonistic, recent
535 studies suggest that such antagonism might have been evolutionary acquired after the split of
536 gymnosperms and angiosperms (de Vries et al., 2018). Our comparative analysis of the

537 transcriptional changes in response to TMV infection in Marchantia and those found in response
538 to treatments with Salicylic and jasmonates (dn-OPDA), as well as in Mpjaz-1 KO plants, show
539 that both SA and jasmonates pathways might contribute to the activation of genes involved in
540 phenylpropanoid metabolism. Those findings are in line with Salicylic and jasmonates triggering
541 this very same pathway in the moss *Physcomitrium patens,* which in turn is responsible for the
542 production of defense-related compounds. (de Vries et al., 2018). Likewise, in line with their
543 synergistic interaction is responsible for local and systemic resistance against TMV in *Nicotiana*
544 *benthamiana* (Zhu et al., 2014), both salicylic and jasmonates activate genes involved in antiviral
545 defense responses that are also responsive to TMV infection in Marchantia. Finally, a set of
546 SA/dn-OPDA commonly upregulated genes might contribute to the above mentioned sustained
547 wound response, and therefore, to contain virus spread.

548 Our work also highlights the conservation of central players, such as MpNAC7, in the specific
549 defense against TMV. Future research might focus on comparative studies to ascertain the
550 conservation of the genetic networks under MpNAC7 and ATAF2 regulation both in Marchantia
551 and Arabidopsis.

552 Collectively, results from this work suggest the presence of evolutionary conserved and divergent
553 plant strategies to cope with viral infections. Those might include gain and loss of defense
554 strategies, such as those involving wound responses. Evolution of plant-virus interactions might
555 also encompass the gradual acquisition of new elements within the underlying gene networks,
556 as those physically interacting with pathogen-derived proteins. Finally, defense mechanisms
557 might undergo anatomical re-location to newly pathogen-targeted cell-types and tissues over
558 evolutionary times.

559

560 **Material and methods**

561 *Plant growth conditions*

562 Male *Marchantia polymorpha* plants Takaragaike-1 (Tak-1) were grown on plates with half
563 strength Gamborg´s B5 medium (Duchefa) containing 1% agar and 1% sucrose under continuous
564 light and 22ºC.

565 *Nicotiana benthamiana* plants were grown on soil under long day conditions (16h light/ 8h dark)
566 and 25ºC.

567 Arabidopsis thaliana plants were grown on soil under long day conditions and 23 ºC.

568 *Infection assays*

569 Frozen tissue from Marchantia plants from the Tübingen population or lab grown Tak-1 plants
570 was homogenized in liquid nitrogen cold mortars, resuspended in phosphate buffer pH7.2,
571 filtered using 70 µM filters and kept at 4ºC. Two-week old Tak-1 plants grown in sterile conditions
572 in plates were vacuum incubated with each of both extracts and transferred to plates containing
573 wet soil. Eight Tak-1 individuals exposed to each sap were collected either one or two weeks
574 after incubation to assess viral replication.

575 Two weeks-old *Nicotiana benthamiana* plants were infiltrated with an agrobacterium solution
576 (0.5 O.D) carrying the TMV-GFP clone (Peart et al., 2002). Infected Nicotiana plants were grown
577 for 3 additional weeks along with non-infected plants and upper leaves displaying infection
578 symptoms were collected, along with equivalent ones from non-infected plants and frozen in
579 liquid nitrogen. Subsequently, leaf tissue was grinded in a liquid nitrogen cold mortar. Sap was
580 isolated from grinded leaf tissue using phosphate buffer pH 7.2, filtered with 70 µM filters and
581 maintained at 4ºC. Two-weeks old Tak-1 plants were incubated either in TMV-GFP containing sap
582 or sap from non-infected plants (mock) for 5 minutes in vacuum. After incubation, Tak-1 plants
583 were transferred to plates containing wet soil and brought back to the growth chamber. GFP
584 signal was monitored 1 and 2 weeks after incubation using a portable UV lamp or with a
585 magnifying stereoscope couple to a UV light source.

586 *RNA isolation and expression analysis*

587 Total RNA was extracted from Marchantia plants and Arabidopsis inflorescences using the
588 protocol described in (Box et al., 2011). Marchantia isolated RNA was further cleaned using the
589 RNeasy Kit (Qiagen). 500 ngs of total RNA were DNase I treated (Fisher Scientific) and converted
590 into cDNA using the RevertAid first strand kit (Fisher Scientific) following the manufacturer
591 instructions. RT-qPCR experiments were performed in a lightcycler (ROCHE) device. Relative
592 expression changes were calculated using the $2^{-\Delta\Delta Ct}$ method using *MpACTIN7* (Mp6g11010) gene
593 as housekeeping. Primers utilized can be found in supplementary table 14.

594 *RNA-seq analysis*

595 For virome studies, 1 µg of total RNA from each of the 21 individuals included in the study was
596 pooled and 4 µg from the mixture were used for preparing two independent libraries using total

597 ribo-depleted RNA following the manufacturer instructions (Illumina TruSeq Stranded total RNA
598 LT sample prep Kit, plant). The first library containing samples from 14 individuals wassequenced
599 on an Illumina NovaSeq 6000 device in 2x150 bp mode, while the second one containing RNA
600 from 7 individuals, was sequenced in an Illumina NovaseqX device. A total of 306,895,552 and
601 506,670,250 reads were respectively obtained. The reads were trimmed and further analysed
602 using QIAGEN CLC Genomics Workbench 21 (https://digitalinsights.qiagen.com/). Dataset was
603 analysed for the presence of known and new viruses using an established virus detection
604 pipeline (Pecman et al., 2017), which includes: reads trimming, *de novo* assembly of trimmed
605 reads, mapping of reads and contigs to NCBI viral RefSeq database (search for known viruses)
606 and pFam domain search for contig sequences (search for known and unknown viruses). To
607 detect known viruses, results of reads mapping to viral RefSeq database were inspected and
608 filtered for viruses for which at least 1000 nts of the reference sequence were covered by
609 mapped reads (Supplementary table 1). In parallel, to detect known viruses and search for new
610 ones, results of the pFam domain search of contig sequences were filtered for hits to viral
611 proteins. Then, this candidate list of viral contigs was additionally queried for similarity against
612 complete NCBI *nr* database (October 2020) using blastx (Gish and States, 1993) and the similarity
613 search results were visualized and taxonomically classified using MEGAN 6 (Huson et al., 2016b).
614 Contigs corresponding to cellular organisms in this analysis were excluded from the list to obtain
615 a final list of putative viral-like sequences (Supplementary table 2). Trimmed sequencing reads
616 were mapped to the list of putative viral-like sequences, to estimate the abundance of
617 corresponding nucleic acids in the sequenced sample and the results were reported as average
618 mapping depth (number of times a position is covered by sequencing reads, averaged over a
619 complete contig length; Supplementary table 2).

620 The presence of selected viruses (three new and two known) was tested by RT-qPCR in RNA
621 extracts of collected samples as described above and datamining approach was used to search
622 for association of those viruses with different sample types linked with publicly available short
623 read datasets. This was performed by querying Serratus infrastructure palmprint database
624 (Edgar et al., 2022) by RdRp sequences of selected viruses using palmID tool
625 (https://serratus.io/palmid).

626 For a newly discovered picorna-like virus, named Tübingen picorna-like virus 1, additional
627 analyses were performed, aiming to ascertain its association with *M. polymorpha*. Putative
628 protein domains were annotated on the viral genome by InterProScan search

629 (https://www.ebi.ac.uk/interpro/search/sequence/, May 2024) of the two discovered open
630 reading frames against all included databases. Amino acid sequence of ORF 1 of the virus
631 (containing RNA-dependent polymerase (RdRp) domain) was queried for similarity against
632 complete NCBI *nr* database (January 2022) using blastp. Fifteen best hits according to bit score
633 values (which have at least 33% identity with the conserved part of the RdRp domain of the
634 queried virus) were included into phylogenetic analysis. Alignment of the sequences of the
635 conserved part of RdRp was performed using MAFFT 7.48 (Katoh and Standley, 2013), followed
636 by alignment trimming using TrimAI 1.3 in Automated 1 mode (Capella-Gutiérrez et al., 2009).
637 Then, best protein substitution model was selected using Model Finder (Kalyaanamoorthy et al.,
638 2017) and maximum likelihood phylogenetic tree inference was performed based on the
639 trimmed alignment using IQ-Tree 1.6.12 (Nguyen et al., 2015), using 1000 ultrafast bootstrap
640 replicates (Hoang et al., 2018). The resulting phylogenetic tree was visualized using iTOL 6.5
641 (Letunic and Bork, 2021) and viral taxa on the tree were coloured according to the associated
642 sample source, as designated in NCBI GenBank. To obtain even more in-depth information about
643 the phylogenetic position of the newly discovered virus, its sequence was aligned also against
644 members of the most related family-level cluster of RdRp sequences (f.0032) from RNA Viruses
645 in Metatranscriptomes (RVMT) database (https://riboviria.org/) (Neri et al., 2022). Alignment
646 and phylogenetic analyses were performed as described above, excluding TrimAI step.

647 For analysing the transcriptional response in Marchantia plants to TMV infection, 1 ug of total
648 RNA was used for preparing each stranded library by mRNA enrichment following manufacturer
649 indications (TrueSeq kit from Illumina). Libraries were sequenced on a Novaseq 6000 device. A
650 total of 20-21 million pairs were obtained per sample. Adapter removal and trimming of low
651 quality bases was done using Trim Galore! v0.6.1
652 (https://www.bioinformatics.babraham.ac.uk/projects/trim_galore/), removing reads shorter
653 than 20 bps and non-paired reads after the trimming step. Ribosomal RNA reads were removed
654 using SortMeRNA v2.1b (Kopylova et al., 2012), removing also reads that become unpaired after
655 this filtering step.

656 Cleaned reads together with the transcriptome of *Marchantia polymorpha* were used to quantify
657 gene expression at transcript level using Salmon v1.1.0 (Patro et al., 2017).

658 For this, the file MpTak1v5.1_r1.mrna.fasta containing the Marchantia transcriptome (v5.1) was
659 downloaded from https://marchantia.info/download/tak1v5.1/ (as of 19-Jan-2021). This file was
660 indexed using *Salmon index* and then used as input for *Salmon quant*, which was ran with

661 parameters -l A, –validateMappings, --recoverOrphans, --rangeFactorizationBins 4, --seqBias,
662 and –gcBias. Mapping rate was found to be in the 89.5%-92.58% range.

663 The R progam tximport v1.14.2 (Soneson et al., 2015) was used to aggregate Salmon's transcript
664 expression estimates at gene level and the *DESeqDataSetFromTximport* from the R package
665 DESeq2 v1.26.0 (Love et al., 2014) was used to create an R object with count data and
666 experimental information for all samples. A low-expression filter was then applied to remove any
667 gene with less than 10 counts across all 8 analyzed samples, resulting in a final set of 14,980
668 genes (from 19,217 annotated genes). Then, the *DESeq* function, which, among other things,
669 computes size factors for sample normalization, was applied to the filtered object. DESeq2's *rlog*
670 function was used to transform count data to the log2 scale while minimizing for differences
671 between samples for low-expressed genes. The transformed data was fed to DESeq2's *plotPCA*
672 function to visualize a PCA plot of the samples.

673 The analysis of differential expression was done using DESeq2's *results* function with the filtered
674 and normalized object as input and parameter *alpha = 0.05.*

675 All datasets used in this study for comparative analysis (wound response and salicylic acid time
676 course) were analysed in the very same way as described above.

677 All Gene ontology analysis (GO) were performed using PLAZA
678 (https://bioinformatics.psb.ugent.be/plaza/). Redundancy on representative categories was
679 reduced using Revigo (http://revigo.irb.hr/).

680 For correlation analysis of transcriptome responses between developmental trajectories and
681 TMV response, raw reads were processed as described above, except that rRNA was removed
682 using ribodetector_cpu v0.2.7 (Deng et al., 2022) and Salmon version was v1.9.0. Salmon's
683 counts were converted into a DESeq2 object and a low-expression filter was applied as described
684 above. Next, the existing batch effect between time course samples and sliced tissue ones was
685 removed using the Combat seq function from the sva package (Leek et al., 2023), v3.48.0. Then,
686 values for biological replicates were averaged and Pearson correlation was computed for the
687 resulting count matrix and displayed using the Heatmap function from the ComplexHeatmap
688 package (Gu, 2022). The batch correction, correlation and heatmap plotting steps were based
689 on the R script used in (Wang et al., 2023) and kindly provided by the authors.

690 *DNA-seq data mining*

691 Data mining was utilized to search for possible DNA viruses associated with *M. polymorpha.*
692 DNA-seq data from a recent study of *M. polymorpha* from natural populations (Beauliue et al.,
693 2023) was retrieved from the SRA database (BioProject PRJNA931118). 74 biosample accessions
694 were selected to encompass diverse geographical locations and various *M. polymorpha*
695 subspecies. Datasets were analyzed using a customized pipeline for virus detection, designed
696 with the Snakemake workflow management system (v.7.32.4) (Köster et al., 2021). Some of the
697 chosen accessions contained sequencing data from multiple runs, which were merged before
698 analysis. The downloaded reads were processed using a custom script: (available at:
699 https://github.com/LanaVogrinec/snakemake-marchantia). Briefly, reads were trimmed with
700 trimmomatic (v.0.39) (Bolger et al., 2014) and assembled into contigs with MEGAHIT (v.1.2.9) (Li
701 et al., 2015). A similarity search was performed against the NCBI *nr* database (February 2024)
702 using DIAMOND (v.0.9.14) blastx (Buchfink et al., 2015) and the hits were taxonomically classified
703 with MEGAN6 (v.6.25.9) (Huson et al., 2016). Contig sequences classified as viral (group 'Viruses'
704 in MEGAN analysis) were extracted and are available, together with their classifications, in
705 Supplementary Table 6.

706 *sRNA library construction and data processing*

707 TMV-GFP positive areas were collected from 2 Marchantia plants infected for 2 weeks in two
708 biological replicates. RNA was isolated following the protocol described in (Box et al., 2011). 10
709 ngs of total RNA were used to build two independent libraries following manufacturer indications
710 (RealSeq-AC, Somagenics). Libraries were sequenced in an Illumina NovaSeq device. A total of
711 26-35 million single-end reads (101 bp) were obtained per sample. Adapter removal and
712 trimming of low quality bases was done using Trim Galore! v0.6.1
713 (https://www.bioinformatics.babraham.ac.uk/projects/trim_galore/) with parameters *-q 15 --*
714 *clip_R1 1 --length 16*.

715 Cleaned reads were then mapped to the TMV-GFP sequence using hisat2 (v2.1.0, (Kim et al.,
716 2019)) with default parameters. The resulting sam files were sorted and indexed using Samtools
717 (v1.15.1, (Danecek et al., 2021)) and the length distribution of reads mapping to the TMV-GFP
718 sequence was computed using samtools stats.

719
720 *Constructs and plant transformation*

721 cDNA from Marchantia mock treated plants was used to amplify the coding regions of *MpTOM1*
722 (Mp3g00660), *MpGDI2* (Mp6g05010) and *MpNAC7* (Mp6g02620) by PCR using Phusion
723 polymerase (NEB). Arabidopsis *Bobber1* (At5g53400) and *ATAF2* (At5g08790) were amplified
724 using cDNA synthesized from RNA from Arabidopsis inflorescences. p126 and Δp126 were
725 amplified using DNA from the TMV-GFP containing plasmid. All obtained fragments were further
726 incubated with dATP and Taq DNA polymerase (NEB) for 1 hour before cloned into the gateway
727 compatible vector PCR8/GW/TOPO TA (Invitrogen) or directly cloned to pENTR D-TOPO
728 (Invitrogen) in the case of ATAF2. An entry vector containing the Arabidopsis AGO1 was kindly
729 provided by Pablo Manavella. Inserts were cloned into their final vectors through LR reaction
730 using LR clonase II (Invitrogen). All plasmids were submitted to Sanger sequencing to corroborate
731 their integrity before used in the corresponding experiments. A list of used primers and
732 constructs can be found in supplementary table 14 and supplementary table 15.

733 Plant transformation was performed as described in (Ishizaki et al., 2008)and selected in
734 Gamborg´s B5 media supplemented with Kanamycin 100mg/ml and Cefotaxime 100mg/ml.

735 *Histology and imaging*

736 Marchantia plants were embedded in 8% agarose and cross-sections of around 200 µM were
737 obtained using a vibratome. Confocal imaging was performed using Leica SP5. Images were
738 processed using Fiji (Schindelin et al., 2012).

739 *Protein-protein interaction assays*

740 Interactions in the yeast two-hybrid system was assayed on selective medium (L^-, W^-, H^-). The
741 assay was repeated 3 times. For the luciferase complementation assay, one-month old rdr6i
742 Nicotiana plants were used. *Agrobacterium tumefaciens* cultures with the different constructs
743 were mixed in the same amounts at a final OD_{600}=0.6. Leaves were imaged three days after
744 inoculation using a LAS4000 device.

745 *Photosynthetic measurements*

746 10 infected and 10 mock treated plants were subjected to 10 measures each using a IMAGING-
747 PAM Maxi device (Heinz Walz GmbH). Quantification was done using the ImagingWing integrated
748 software.

749 **Acknowledgments**

750 We would like to thank Juan Jose López-Moya, Miguel A. Blázquez and Salomé Prat for critical
751 reading of the manuscript. Sebastian Schornack, Phil Carella, Alexander Summers, the CUBG
752 curation team (Samuel Brockington and Mar Millan), Klaus Schlaeppi, Katja Rembold, Alba
753 Gonzalez, Detlef Weigel, Alexandra Kehl, Brigitte Fiebig, Luisa Lanfranco, Mara Novero, Isabel
754 Monte, Adrián Vojtassák, Sabine Zachgo and Claudia Gieshoidt for their help in obtaining
755 Marchantia individuals for the virome assays. Neža Pajek Arambašić for help with pipeline
756 automation. We would like to thank Eduardo Bejarano for providing the plasmid containing TMV-
757 GFP and Antonio Darós for providing TuMV-ROS1 and TMV-ROS1 containing plasmids. Pablo
758 Manavella for the AtAGO1-pEntr plasmid. Phil Carella for an updated annotation of NLR genes in
759 Marchantia. We would also thank to Jia-Wei Wang, Long Wang and Jie Xu for sharing the code
760 used for correlation analysis between TMV transcriptional responses and the different samples
761 from Marchantia developmental trajectories.

762 The work in the MoRE lab is funded by RYC-2015-19154 (funded by MCIN/AEI/
763 10.13039/501100011033 and by "ESF Investing in your future"), RTI2018-097262-B-I00 (funded
764 by MCIN/AEI/ 10.13039/501100011033 and by "ERDF A way of making Europe") and through
765 the "Severo Ochoa Programme for Centres of Excellence in R&D" 2016-2019 (SEV-2015-0533)
766 and 2020-2023 (CEX2019-000902-S) funded by MCIN/AEI/ 10.13039/501100011033 and the
767 CERCA programme from the Generalitat de Catalunya to I-R-S. T J-G was recipient of a
768 Postdoctoral Fellowship from CRAG through the "Severo Ochoa Programme for Centres of
769 Excellence in R&D" 2016-2019 (SEV-2015- 0533). L. V-M was supported by BES-2016-076986
770 (funded by MCIN/AEI/ 10.13039/501100011033 and by "ESF Investing in your future"). The work
771 at NIB was funded by Slovenian Research and Innovation Agency core and project financing P4-
772 0407, P4-0165 and J4-4553.

773 Data access: Raw data from the virome has been deposited in SRA and GenBank under Bioproject
774 (PRJNA1022866) and BioSamples (SAMN37631837 and SAMN40978195). Raw data from TMV
775 infected vs. Mock treated plants have been deposit GEO (GSE241827). Reconstructed genomic
776 sequences of three novel viruses uncovered by virome analysis were deposited in NCBI GenBank
777 (OR640980-82).

778 **Figure legends**

779 **Figure 1.** *Marchantia polymorpha is infected by RNA viruses.*

780 (A) Genome structure of Tübingen picorna-like virus 1, newly discovered in composite *M.*
781 *polymorpha* sample with two predicted open reading frames (ORFs) and corresponding
782 average reads mapping depth in sequenced composite sample. Black empty boxes
783 represent predicted protein domains detected by InterProScan: S3H – superfamily 3
784 helicase, 3C-Pro – peptidase C3, RdRp – RNA-dependent RNA polymerase and CP-SJR – coat
785 protein with 8-stranded jelly roll β-barrel motif.

786 (B) Maximum likelihood phylogenetic tree obtained based on the alignment of the
787 conserved part of RdRd of Tübingen picorna-like virus 1 and fifteen other most similar
788 viruses. The tree was midpoint rooted. Coloured virus names correspond to the sources
789 associated with a particular virus, according to the legend on the right side of the panel.
790 Numbers next to the branches represent statistical support (%) of the clades according to
791 the ultrafast bootstrap analysis. Branch length represents the average number of amino acid
792 substitutions per site. Codes next to the taxon names in round brackets are the
793 corresponding NCBI GenBank protein accession numbers. Next to them, fractions in square
794 brackets represent % of identity of Tübingen picorna-like virus 1 to other individual taxons
795 for the aligned part of the RdRp domain.

796 (C) Results of the viral concentration measurements for *M. polmorpha* plants inoculated
797 with Tübingen picorna-like virus 1 positive plant extracts. On the right, relative
798 concentrations of Tübingen picorna-like virus 1 in inoculated plants one- and two-weeks
799 post inoculation are shown; measurements of concentrations in individual plants are shown
800 as dots and the box-whisker plots represent the distribution of values for the two time
801 points (at 1 WPI, x represent an outlier measurement). On the top of the plot, the horizontal
802 connecting line designates statistically significant difference in the means of the two
803 distributions, with the corresponding p-value, according to the nonparametric Wilcoxon
804 rank sum test. Control represents results for Tak-1 incubated plants (N.A. –no virus was
805 detected). BIORENDER was used to prepare this figure.

806 **Figure 2**. *Tobacco mosaic virus replicates in Marchantia plants*.

807 (A) GFP fluorescent signal increases in thalli from 3 week old plants after 1 week, (left panel)
808 compared to thalli from 4 weeks old and 2-weeks infected plants (right panel). Both
809 images show the same part or an infected plant under a magnification device under UV
810 light. Red shows chlorophyll autofluorescence. White bar scale shows 100 µms.

811 (B) TMV-GFP transcripts increase over time in infected plants. Pools of three infected plants
812 were used for each time point. The result from 3 technical replicates is shown. Mock, 4
813 weeks old plants incubated with sap from untreated plants. T0, 2 weeks old plants
814 collected right after incubation with sap from infected plants. T1, 3 weeks old plants
815 collected after 1 week from incubation. T2, 4 weeks old plants collected after 3 weeks
816 from incubation. Expression of TMV is relative to the expression of Marchantia actine.
817 (C) Length distribution of TMV-derived vsRNAs populations found in thalli from 4 weeks old
818 plants after 2 weeks of infection. Nts stans for nucleotides.
819 (D) TMV-GFP infects all cell types. Transversal sections of an Marchantia thalli from a mock
820 treated plant that was 4 weeks old (left) and equivalent area in a plant 2 weeks after
821 infection (right) under confocal image. The pictures show the merge between green (virus)
822 and red (autofluorescence) channels. Merge was performed using Fiji. P stands for
823 Photosynthetic region, S for storage region and E stands for lower epidermis. White bar
824 scale shows 100 µm.

825 **Figure 3.** *TMV triggers stress-related molecular reprogramming in Marchantia.*

826 (A) Set of common PTI marker genes responsive to bacteria and fungal extracts and TMV
827 infection.
828 (B) Set of wound and TMV responsive ERF transcription factors.
829 (C) Venn diagram showing that transcriptional reprogramming upon TMV infection largely
830 overlaps with that found upon wounding.
831 (D) Set of chitin and TMV responsive WRKY transcription factors in Marchantia.
832 (E) Photosynthetic efficiency (Fv/Fm) in infected areas in thalli from 4 weeks old plants after
833 2 weeks of infection compared to equivalent areas from mock treated plants. Statistical
834 assessment was performed using a parametric T-test. Marchantia plants and cameras
835 depicting measured areas come from Biorender. Light green area indicated TMV-GFP
836 positive areas.
837 (F) Photosynthetic efficiency (Fv/Fm) in non-infected areas, in thalli from 4 weeks old plants
838 after 2 weeks of infection, compared to equivalent areas from mock treated plants.
839 Statistical assessment was performed using a parametric T-test. Marchantia plants and
840 cameras depicting measured areas come from Biorender. Light green area indicated
841 TMV-GFP positive areas.

842 **Figure 4**. *Salicylic and jasmonate signalling pathways are activated during Marchantia-TMV*
843 *interaction.*

844 (A) Venn diagrams showing the overlap between the transcriptional responses under TMV
845 infection ad a salicylic treatment time course (2 and 6 hours).
846 (B) Overlap between the trancriptome responses to TMV and Mpjaz1ko mutants with
847 constitutively active jasmonate signalling (left), and treatment with the active dn-OPDA
848 jasmonate (right).
849 (C) Overlap between the trancriptome responses commonly found in TMV infection and the
850 different hormone-related transcriptomes.
851 (D) Biological processes to which genes commonly upregulated in response to TMV infection,
852 SA treatment (2,6 and 12h) and activation of jasmonate signalling belong
853 (E) Biological processes to which genes commonly downregulated in response to TMV
854 infection, SA treatment (12h) and activation of jasmonate signalling belong.
855 (F) Biological processes to which commonly upregulated in response to TMV infection, SA
856 treatment (6 h) and activation of jasmonate signalling in Mpjaz1KO plants belong.
857 (G) Biological processes to which commonly upregulated in response to TMV infection, SA (6 h)
858 and dn-OPDA treatments belong.

859 **Figure 5.** *TMV infection triggers maturation and aging in Marchantia*.

860 (A) Pairwise comparison between transcriptomes from mock and TMV samples along with
861 those from sliced thallus samples. Slice 1(S1) corresponds to the top of thalli (youngest
862 part), while slide 6 (S6), corresponds to the base of thalli encompassing the oldest part.
863 (B) Pairwise comparison between transcriptomes from mock and TMV samples along with
864 those from Marchantia developmental series Day 1 (D1) samples correspond to 1 day
865 after germination (youngest), while day 31 (31D) corresponds to fully mature Marchantia
866 thalli 31 days after germination.

867 **Figure 6.** *Conservation of the interaction between Marchantia and the TMV silencing suppressor*
868 *p126.*

869 (A) P126-GFP shows accumulation in the cytoplasm of Marchantia cells in cross-sections of
870 thalli from 4 weeks old plants (right) compared to thalli from untransformed plants of
871 the same age plants (left). The pictures show the merge between green (GFP) and red
872 (autofluorescence) channels. Merge was performed using Fiji Scale bars are 100 µMs.

873 (B) Overexpression of p126 inhibits growth (area) when compared to Tak-1 control plants.
874 Analysis was done in 4 weeks old plants in 3 biological replicates (n=12). Statistical
875 significance was assessed using a Wilcoxon-test.
876 (C) MpNAC7 interacts with the helicase domain of p126 in yeast.
877 (D) MpNAC7 and ATAF2 interact both with the helicase and the full length p126 in planta.
878 (E) Transient expression of MpNAC7 in Nicotiana plants abrogates local and systemic TMV
879 infection. TMV presence is shown as purple.

880 **Supplementary figure 1**. Phylogenetic position of a newly discovered Tübingen picorna-like virus
881 1 in regard to the most related RNA-dependent RNA polymerase (RdRp) sequences from RNA
882 Viruses in Metatranscriptomes (RVMT) database (https://riboviria.org/).

883 (A) Maximum likelihood phylogenetic tree obtained based on the alignment of the RdRd of
884 Tübingen picorna-like virus 1 and 476 sequences corresponding to f.0032 cluster (within
885 Picornavirales) from RVMT database. The tree was midpoint rooted. Tübingen picorna-
886 like virus 1 is designated by green arrow. Ultrafast bootstrap support (>90%) is shown as
887 circles according to the legend on the left. Branch length represents the average number
888 of amino acid substitutions per site. Leaf labels represent RdRp sequences from RVMT
889 database with additional info given in Supplementary table #.
890 (B) A pruned phylogenetic tree from (A) showing in detail the clade containing RdRp
891 sequences most similar to Tübingen picorna-like virus 1 (red box in (A)). Source sample
892 environments linked with those RdRp sequences in RVMT database are shown in round
893 brackets, with additional info given in Supplementary table #. Numbers next to the
894 branches represent statistical support (%) of the clades according to the ultrafast
895 bootstrap analysis.

896 **Supplementary figure 2.** *Nicotiana benthamiana plants inoculated with sap from*
897 *Marchantia infection experiments.*

898 (A) Nicotiana plants inoculated with sap from mock treated plants. Upper panel, top view
899 of plant with white light. Down panel, same Nicotiana plant under UV light. Scale bars
900 signify 1 cm.
901 (B) Nicotiana plants inoculated with sap from TMV-GFP treated plants. Upper panel, top
902 view of plant with white light showing crinkled and yellowish leaves as result of TMV

903 infection. Down panel, same Nicotiana plant under UV light showing GFP signal from
904 TMV infection in leaves showing symptoms. Scale bars signify 1 cm.
905 (C) Inset from a TMV-GFP infected leaf showing symptoms of infection (reduced chlorophyll
906 content) in the upper panel, coinciding with TMV-derived GFP signal under UV light.
907 Scale bars signify 1 cm.

908 **Supplementary figure 3.** *TMV infections progress in Marhantia thalli over time.*

909 Thalli from Marchantia plants showing the progression of TMV infection inferred by GFP signal.
910 Left, 3 weeks old plant after 1 week inoculation. Right, 4 weeks old plant after 2 weeks
911 inoculation. Additional replicate to that shown in Figure 2A.

912 **Supplementary figure 4.** *TMV replicates in Marchantia plants.*

913 Two additional biological replicates to the one shown in Figure 2B. Whole individuals were
914 collected in pools of 3 for each time point. Mock, 4 weeks old plants incubated with sap from
915 untreated plants. T0, 2 weeks old plants collected right after incubation with sap from infected
916 plants. T1, 3 weeks old plants collected after 1 week from incubation. T2, 4 weeks old plants
917 collected after 3 weeks from incubation. Expression of TMV is relative to the expression of
918 Marchantia actine.

919 **Supplementary figure 5.** *Marchantia infected thalli accumulate TMV-derived vsRNAs.*

920 (A). Length distribution of TMV-derived vsRNAs profiled by sRNA sequencing showing that the
921 predominant population belong to 21 nts long consistent with the absence of DCL2 and the
922 presence of DCL4 in the Marchantia´s genome. Data shown belongs to replicate 2, being replicate
923 1 that shown in Figure 2B. Nts stans for nucleotides.

924 (B). Mapping of vsRNAs to the TMV-GFP sequence from both Replicate 1 (Figure 2B) and
925 Replicate 2 (Sup. Figure 5A).

926 **Supplementary figure 6**. *Sampling and validation of samples for transcriptomic assays.*

927 (A) Example of areas collected from mock, upper panel, and TMV-GFP infected plants for
928 transcriptomic assays. Scale bars signify 1 cm.
929 (B) RT-qPCR validation of TMV-GFP levels in the 4 pools used for RNA-seq.
930 (C) Principal component analysis of the different replicates from RNA-seq experiment.

931 **Supplementary figure 7.** *Gene ontology analysis of biological processes to which DEGs in respond*
932 *to TMV infection belong.*

933 (A) GO categories from upregulated genes in response to TMV infection.
934 (B) Selected GO categories from downregulated genes in response to TMV infection.

935 **Supplementary figure 8.** *Overlap between DEGs responding to 12 hours of incubation in salicylic*
936 *acid and those responsive TMV infection.*

937 **Supplementary figure 9.** P126 overexpression results in reduced growth.

938 Representative 4 weeks old individuals from the phenotypic assay presented in Figure 6B. Scale
939 bars represent 1 cm.

940 **Supplementary figure 10.** *MpNAC7 specifically abrogates TMV infection in Nicotiana plants.*

941 (A) Picture of inoculated leaves showing that MpNAC7 abrogates local TMV but not turnip
942 mosaic virus (TuMV) infection (purple colour).
943 (B) Effect in systemic leaves.
944 (C) Upper view of infected plants.

945

946 **Supplementary table 1.** *Detection of viral sequences of known viruses*.

947 **Supplementary table 2.** *Detection of known and putative novel virus-like sequences*.

948 **Supplementary table 3.** *Demographic study for the presence of a set of known and newly*
949 *identified virus in individuals from the different sampling sites*.

950 **Supplementary table 4.** *Results of the palmID scan (https://serratus.io/palmid) for set of known*
951 *and newly identified viruses.*

952 **Supplementary table 5.** *Metadata for RdRp clusters showed on Supplementary figure 1.*

953 **Supplementary table 6.** *Results of the mining of DNA sequencing data (BioProject PRJNA931118)*
954 *for the presence of known and putative novel viral sequences.*

955 **Supplementary table 7.** *List of DEG in response to TMV infection in Marchantia.*

956 **Supplementary table 8.** *List of Pathogenesis-related (PR) genes differentially expressed upon*
957 *TMV infection.*

958 **Supplementary table 9.** *List of NLR genes differentially expressed upon TMV infection.*

959 **Supplementary table 10.** *List of GO categories of the biological processes to which upregulated*
960 *genes in response to TMV infection belong.*

961 **Supplementary table 11.** *List of GO categories of the biological processes to which*
962 *downregulated genes in response to TMV infection belong.*

963 **Supplementary table 12.** *List of GO categories of the biological processes to which commonly*
964 *responsive genes to TMV infection and salicylic acid time course treatment, Mpjaz-1ko mutants*
965 *and dn-OPDA treatment belong.*

966 **Supplementary table 13.** *List of GO categories of the biological processes to which commonly*
967 *responsive genes to TMV infection and different hormone-related transcriptomes belong.*

968 **Supplementary table 14.** *Table of primers used in this study.*

969 **Supplementary table 15.** *Table of constructs used in this study.*

970

971 **Bibliography:**

972 BALLY, J., NAKASUGI, K., JIA, F., JUNG, H., HO, S. Y., WONG, M., PAUL, C. M., NAIM, F., WOOD, C.
973 C., CROWHURST, R. N., HELLENS, R. P., DALE, J. L. & WATERHOUSE, P. M. 2015. The
974 extremophile Nicotiana benthamiana has traded viral defence for early vigour. *Nat*
975 *Plants,* 1**,** 15165.
976 BEAULIEU, C., LIBOUREL, C., ZAMAR, D. L. M., MAHBOUBI, K. EL, HOEY, D. J., KELLER, J., GIROU,
977 C., CLEMENTE, H. S., DIOP, I., AMBLARD, E., THÉRON, A., CAUET, S., RODDE, N., ZACHGO,
978 S., HALPAPE, W., MEIERHENRICH, A., LAKER, B., BRAUTIGAM, A., GREIFF, G. R., …
979 DELAUX, P.-M. 2023. The Marchantia pangenome reveals ancient mechanisms of plant
980 adaptation to the environment. *BioRxiv*, *8*(7), 2023.10.27.564390.
981 https://doi.org/10.1101/2023.10.27.564390
982 BECK, M., WYRSCH, I., STRUTT, J., WIMALASEKERA, R., WEBB, A., BOLLER, T. & ROBATZEK, S. 2014.
983 Expression patterns of flagellin sensing 2 map to bacterial entry sites in plant shoots and
984 roots. *J Exp Bot,* 65**,** 6487-98.
985 BEDOYA, L. C., MARTINEZ, F., ORZAEZ, D. & DAROS, J. A. 2012. Visual tracking of plant virus
986 infection and movement using a reporter MYB transcription factor that activates
987 anthocyanin biosynthesis. *Plant Physiol,* 158**,** 1130-8.
988 BELANGER, S., ZHAN, J. & MEYERS, B. C. 2023. Phylogenetic analyses of seven protein families
989 refine the evolution of small RNA pathways in green plants. *Plant Physiol,* 192**,** 1183-
990 1203.
991 BENITEZ, M., HERNANDEZ-HERNANDEZ, V., NEWMAN, S. A. & NIKLAS, K. J. 2018. Dynamical
992 Patterning Modules, Biogeneric Materials, and the Evolution of Multicellular Plants.
993 *Front Plant Sci,* 9**,** 871.

994 BOLGER, A. M., LOHSE, M. & USADEL, B. 2014. Trimmomatic: a flexible trimmer for Illumina
995 sequence data. *Bioinformatics,* 30**,** 2114-20.
996 BOWLES, A. M. C., PAPS, J. & BECHTOLD, U. 2022. Water-related innovations in land plants
997 evolved by different patterns of gene cooption and novelty. *New Phytol,* 235**,** 732-742.
998 BOWMAN, J. L., KOHCHI, T., YAMATO, K. T., JENKINS, J., SHU, S., ISHIZAKI, K., YAMAOKA, S.,
999 NISHIHAMA, R., NAKAMURA, Y., BERGER, F., ADAM, C., AKI, S. S., ALTHOFF, F., ARAKI, T.,
1000 ARTEAGA-VAZQUEZ, M. A., BALASUBRMANIAN, S., BARRY, K., BAUER, D., BOEHM, C. R.,
1001 BRIGINSHAW, L., CABALLERO-PEREZ, J., CATARINO, B., CHEN, F., CHIYODA, S., CHOVATIA,
1002 M., DAVIES, K. M., DELMANS, M., DEMURA, T., DIERSCHKE, T., DOLAN, L., DORANTES-
1003 ACOSTA, A. E., EKLUND, D. M., FLORENT, S. N., FLORES-SANDOVAL, E., FUJIYAMA, A.,
1004 FUKUZAWA, H., GALIK, B., GRIMANELLI, D., GRIMWOOD, J., GROSSNIKLAUS, U.,
1005 HAMADA, T., HASELOFF, J., HETHERINGTON, A. J., HIGO, A., HIRAKAWA, Y., HUNDLEY, H.
1006 N., IKEDA, Y., INOUE, K., INOUE, S. I., ISHIDA, S., JIA, Q., KAKITA, M., KANAZAWA, T.,
1007 KAWAI, Y., KAWASHIMA, T., KENNEDY, M., KINOSE, K., KINOSHITA, T., KOHARA, Y., KOIDE,
1008 E., KOMATSU, K., KOPISCHKE, S., KUBO, M., KYOZUKA, J., LAGERCRANTZ, U., LIN, S. S.,
1009 LINDQUIST, E., LIPZEN, A. M., LU, C. W., DE LUNA, E., MARTIENSSEN, R. A., MINAMINO,
1010 N., MIZUTANI, M., MIZUTANI, M., MOCHIZUKI, N., MONTE, I., MOSHER, R., NAGASAKI,
1011 H., NAKAGAMI, H., NARAMOTO, S., NISHITANI, K., OHTANI, M., OKAMOTO, T.,
1012 OKUMURA, M., PHILLIPS, J., POLLAK, B., REINDERS, A., ROVEKAMP, M., SANO, R., SAWA,
1013 S., SCHMID, M. W., SHIRAKAWA, M., SOLANO, R., SPUNDE, A., SUETSUGU, N., SUGANO,
1014 S., SUGIYAMA, A., SUN, R., SUZUKI, Y., TAKENAKA, M., et al. 2017. Insights into Land Plant
1015 Evolution Garnered from the Marchantia polymorpha Genome. *Cell,* 171**,** 287-304 e15.
1016 BOX, M. S., COUSTHAM, V., DEAN, C. & MYLNE, J. S. 2011. Protocol: A simple phenol-based
1017 method for 96-well extraction of high quality RNA from Arabidopsis. *Plant Methods,* 7**,**
1018 7.
1019 BRANTS, D. H. 1961. The Influence of Meristematic Tissue and Injuries on the Transport of
1020 Tobacco Mosaic Virus in Nicotiana tabacum L. cultivar. Samsun. *Acta Botanica*
1021 *Neerlandica,* 10**,** 113-163.
1022 BUCHFINK, B., XIE, C. & HUSON, D. H. 2015. Fast and sensitive protein alignment using DIAMOND.
1023 *Nat Methods,* 12**,** 59-60.
1024 BUTKOVIC, A., DOLJA, V. V., KOONIN, E. V. & KRUPOVIC, M. 2023. Plant virus movement proteins
1025 originated from jelly-roll capsid proteins. *PLoS Biol,* 21**,** e3002157.
1026 CAMPBELL, R. N. 1996. Fungal transmission of plant viruses. *Annu Rev Phytopathol,* 34**,** 87-108.
1027 CAPELLA-GUTIÉRREZ, S., SILLA-MARTÍNEZ, J. M. & GABALDÓN, T. 2009. trimAl: a tool for
1028 automated alignment trimming in large-scale phylogenetic analyses. *Bioinformatics,* 25**,**
1029 1972-1973.
1030 CARELLA, P., GOGLEVA, A., HOEY, D. J., BRIDGEN, A. J., STOLZE, S. C., NAKAGAMI, H. &
1031 SCHORNACK, S. 2019. Conserved Biochemical Defenses Underpin Host Responses to
1032 Oomycete Infection in an Early-Divergent Land Plant Lineage. *Curr Biol,* 29**,** 2282-2294
1033 e5.
1034 CARELLA, P., GOGLEVA, A., TOMASELLI, M., ALFS, C. & SCHORNACK, S. 2018. Phytophthora
1035 palmivora establishes tissue-specific intracellular infection structures in the earliest
1036 divergent land plant lineage. *Proc Natl Acad Sci U S A,* 115**,** E3846-E3855.
1037 CHIA, K.-S., KOURELIS, J., VICKERS, M., SAKA, I. T., KAMOUN, S. & CARELLA, P. 2022. The N-
1038 terminal executioner domains of NLR immune receptors are functionally conserved
1039 across major plant lineages. *bioRxiv*.
1040 CHIA, K. S., KOURELIS, J., TEULET, A., VICKERS, M., SAKAI, T., WALKER, J. F., SCHORNACK, S.,
1041 KAMOUN, S. & CARELLA, P. 2024. The N-terminal domains of NLR immune receptors
1042 exhibit structural and functional similarities across divergent plant lineages. *Plant Cell*.

1043 COLLUM, T. D. & CULVER, J. N. 2017. Tobacco mosaic virus infection disproportionately impacts
1044 phloem associated translatomes in Arabidopsis thaliana and Nicotiana benthamiana.
1045 *Virology,* 510**,** 76-89.
1046 DANECEK, P., BONFIELD, J. K., LIDDLE, J., MARSHALL, J., OHAN, V., POLLARD, M. O., WHITWHAM,
1047 A., KEANE, T., MCCARTHY, S. A., DAVIES, R. M. & LI, H. 2021. Twelve years of SAMtools
1048 and BCFtools. *Gigascience,* 10.
1049 DE VRIES, S., DE VRIES, J., VON DAHLEN, J. K., GOULD, S. B., ARCHIBALD, J. M., ROSE, L. E. &
1050 SLAMOVITS, C. H. 2018. On plant defense signaling networks and early land plant
1051 evolution. *Commun Integr Biol,* 11**,** 1-14.
1052 DEBAT, H., GARCIA, M. L. & BEJERMAN, N. 2023. Expanding the Repertoire of the Plant-Infecting
1053 Ophioviruses through Metatranscriptomics Data. *Viruses,* 15.
1054 DELESSERT, C., KAZAN, K., WILSON, I. W., VAN DER STRAETEN, D., MANNERS, J., DENNIS, E. S. &
1055 DOLFERUS, R. 2005. The transcription factor ATAF2 represses the expression of
1056 pathogenesis-related genes in Arabidopsis. *Plant J,* 43**,** 745-57.
1057 DENG, Z. L., MUNCH, P. C., MRECHES, R. & MCHARDY, A. C. 2022. Rapid and accurate
1058 identification of ribosomal RNA sequences via deep learning. *Nucleic Acids Res,* 50**,** e60.
1059 DING, S. W., HAN, Q., WANG, J. & LI, W. X. 2018. Antiviral RNA interference in mammals. *Curr*
1060 *Opin Immunol,* 54**,** 109-114.
1061 DING, S. W. & VOINNET, O. 2007. Antiviral immunity directed by small RNAs. *Cell,* 130**,** 413-26.
1062 DING, X. S., LIU, J., CHENG, N. H., FOLIMONOV, A., HOU, Y. M., BAO, Y., KATAGI, C., CARTER, S. A.
1063 & NELSON, R. S. 2004. The Tobacco mosaic virus 126-kDa protein associated with virus
1064 replication and movement suppresses RNA silencing. *Mol Plant Microbe Interact,* 17**,**
1065 583-92.
1066 DOLJA, V. V., KRUPOVIC, M. & KOONIN, E. V. 2020. Deep Roots and Splendid Boughs of the Global
1067 Plant Virome. *Annu Rev Phytopathol,* 58**,** 23-53.
1068 DOS REIS FIGUEIRA, A., GOLEM, S., GOREGAOKER, S. P. & CULVER, J. N. 2002. A nuclear
1069 localization signal and a membrane association domain contribute to the cellular
1070 localization of the Tobacco mosaic virus 126-kDa replicase protein. *Virology,* 301**,** 81-9.
1071 EDGAR, R. C., TAYLOR, B., LIN, V., ALTMAN, T., BARBERA, P., MELESHKO, D., LOHR, D.,
1072 NOVAKOVSKY, G., BUCHFINK, B., AL-SHAYEB, B., BANFIELD, J. F., DE LA PENA, M.,
1073 KOROBEYNIKOV, A., CHIKHI, R. & BABAIAN, A. 2022. Petabase-scale sequence alignment
1074 catalyses viral discovery. *Nature,* 602**,** 142-147.
1075 ERICKSON, F. L., HOLZBERG, S., CALDERON-URREA, A., HANDLEY, V., AXTELL, M., CORR, C. &
1076 BAKER, B. 1999. The helicase domain of the TMV replicase proteins induces the N-
1077 mediated defence response in tobacco. *Plant J,* 18**,** 67-75.
1078 ESPINOZA, C., MEDINA, C., SOMERVILLE, S. & ARCE-JOHNSON, P. 2007. Senescence-associated
1079 genes induced during compatible viral interactions with grapevine and Arabidopsis. *J Exp*
1080 *Bot,* 58**,** 3197-212.
1081 GAN, S. 2003. Mitotic and postmitotic senescence in plants. *Sci Aging Knowledge Environ,* 2003**,**
1082 RE7.
1083 GARCIA-RUIZ, H., TAKEDA, A., CHAPMAN, E. J., SULLIVAN, C. M., FAHLGREN, N., BREMPELIS, K. J.
1084 & CARRINGTON, J. C. 2010. Arabidopsis RNA-dependent RNA polymerases and dicer-like
1085 proteins in antiviral defense and small interfering RNA biogenesis during Turnip Mosaic
1086 Virus infection. *Plant Cell,* 22**,** 481-96.
1087 GIMENEZ-IBANEZ, S., ZAMARRENO, A. M., GARCIA-MINA, J. M. & SOLANO, R. 2019. An
1088 Evolutionarily Ancient Immune System Governs the Interactions between Pseudomonas
1089 syringae and an Early-Diverging Land Plant Lineage. *Curr Biol,* 29**,** 2270-2281 e4.
1090 GISH, W. & STATES, D. J. 1993. Identification of protein coding regions by database similarity
1091 search. *Nat Genet,* 3**,** 266-72.

1092 GU, Z. 2022. Complex Heatmap Visualization. *iMeta*.
1093 GUO, S. & WONG, S. M. 2017. Deep sequencing analysis reveals a TMV mutant with a poly(A)
1094 tract reduces host defense responses in Nicotiana benthamiana. *Virus Res,* 239**,** 126-135.
1095 HERNANDEZ-HERNANDEZ, V., BENITEZ, M. & BOUDAOUD, A. 2020. Interplay between turgor
1096 pressure and plasmodesmata during plant development. *J Exp Bot,* 71**,** 768-777.
1097 HEYMAN, J., CANHER, B., BISHT, A., CHRISTIAENS, F. & DE VEYLDER, L. 2018. Emerging role of the
1098 plant ERF transcription factors in coordinating wound defense responses and repair. *J*
1099 *Cell Sci,* 131.
1100 HOANG, D. T., CHERNOMOR, O., VON HAESELER, A., MINH, B. Q. & VINH, L. S. 2018. UFBoot2:
1101 Improving the Ultrafast Bootstrap Approximation. *Molecular Biology and Evolution,* 35**,**
1102 518-522.
1103 HUSON, D. H., BEIER, S., FLADE, I., GORSKA, A., EL-HADIDI, M., MITRA, S., RUSCHEWEYH, H. J. &
1104 TAPPU, R. 2016a. MEGAN Community Edition - Interactive Exploration and Analysis of
1105 Large-Scale Microbiome Sequencing Data. *PLoS Comput Biol,* 12**,** e1004957.
1106 HUSON, D. H., BEIER, S., FLADE, I., GÓRSKA, A., EL-HADIDI, M., MITRA, S., RUSCHEWEYH, H. J. &
1107 TAPPU, R. 2016b. MEGAN Community Edition - Interactive Exploration and Analysis of
1108 Large-Scale Microbiome Sequencing Data. *Plos Computational Biology,* 12.
1109 ISHIZAKI, K., CHIYODA, S., YAMATO, K. T. & KOHCHI, T. 2008. Agrobacterium-mediated
1110 transformation of the haploid liverwort Marchantia polymorpha L., an emerging model
1111 for plant biology. *Plant Cell Physiol,* 49**,** 1084-91.
1112 IWAMA, R. E. & MORAN, Y. 2023. Origins and diversification of animal innate immune responses
1113 against viral infections. *Nat Ecol Evol,* 7**,** 182-193.
1114 JEON, H.-W., IWAKAWA, H., MARAMOTO, S., HERRFURTH, C., GUSTCHE, N., SCHLÜTER, T.,
1115 KYOZUKA, J., MIYAUCHI, S., FEUSSNER, I., ZACHGO, S. & NAKAGAMI, H. 2022. Contrasting
1116 and conserved roles of NPR pathways in diverged land plant lineages. *bioRxiv*.
1117 JIA, X., WANG, L., ZHAO, H., ZHANG, Y., CHEN, Z., XU, L. & YI, K. 2023. The origin and evolution of
1118 salicylic acid signaling and biosynthesis in plants. *Mol Plant,* 16**,** 245-259.
1119 KALYAANAMOORTHY, S., MINH, B. Q., WONG, T. K. F., VON HAESELER, A. & JERMIIN, L. S. 2017.
1120 ModelFinder: fast model selection for accurate phylogenetic estimates. *Nature*
1121 *Methods,* 14**,** 587-+.
1122 KAPPAGANTU, M., COLLUM, T. D., DARDICK, C. & CULVER, J. N. 2020. Viral Hacks of the Plant
1123 Vasculature: The Role of Phloem Alterations in Systemic Virus Infection. *Annu Rev Virol,*
1124 7**,** 351-370.
1125 KASSCHAU, K. D., XIE, Z., ALLEN, E., LLAVE, C., CHAPMAN, E. J., KRIZAN, K. A. & CARRINGTON, J.
1126 C. 2003. P1/HC-Pro, a viral suppressor of RNA silencing, interferes with Arabidopsis
1127 development and miRNA unction. *Dev Cell,* 4**,** 205-17.
1128 KATOH, K. & STANDLEY, D. M. 2013. MAFFT Multiple Sequence Alignment Software Version 7:
1129 Improvements in Performance and Usability. *Molecular Biology and Evolution,* 30**,** 772-
1130 780.
1131 KIM, D., PAGGI, J. M., PARK, C., BENNETT, C. & SALZBERG, S. L. 2019. Graph-based genome
1132 alignment and genotyping with HISAT2 and HISAT-genotype. *Nat Biotechnol,* 37**,** 907-
1133 915.
1134 KNEESHAW, S., SORIANO, G., MONTE, I., HAMBERG, M., ZAMARRENO, A. M., GARCIA-MINA, J.
1135 M., FRANCO-ZORRILLA, J. M., KATO, N., UEDA, M., REY-STOLLE, M. F., BARBAS, C.,
1136 MICHAVILA, S., GIMENEZ-IBANEZ, S., JIMENEZ-ALEMAN, G. H. & SOLANO, R. 2022.
1137 Ligand diversity contributes to the full activation of the jasmonate pathway in
1138 Marchantia polymorpha. *Proc Natl Acad Sci U S A,* 119**,** e2202930119.

1139 KOONIN, E. V., DOLJA, V. V., KRUPOVIC, M., VARSANI, A., WOLF, Y. I., YUTIN, N., ZERBINI, F. M. &
1140 KUHN, J. H. 2020. Global Organization and Proposed Megataxonomy of the Virus World.
1141 *Microbiol Mol Biol Rev,* 84.
1142 KOPYLOVA, E., NOÉ, L. & TOUZET, H. 2012. SortMeRNA: fast and accurate filtering of ribosomal
1143 RNAs in metatranscriptomic data. *Bioinformatics,* 28**,** 3211-3217.
1144 KORNER, C. J., KLAUSER, D., NIEHL, A., DOMINGUEZ-FERRERAS, A., CHINCHILLA, D., BOLLER, T.,
1145 HEINLEIN, M. & HANN, D. R. 2013. The immunity regulator BAK1 contributes to
1146 resistance against diverse RNA viruses. *Mol Plant Microbe Interact,* 26**,** 1271-80.
1147 KRAMER, S. R., GOREGAOKER, S. P. & CULVER, J. N. 2011. Association of the Tobacco mosaic virus
1148 126kDa replication protein with a GDI protein affects host susceptibility. *Virology,* 414**,**
1149 110-8.
1150 KULSHRESTHA, S., JIBRAN, R., VAN KLINK, J. W., ZHOU, Y., BRUMMELL, D. A., ALBERT, N. W.,
1151 SCHWINN, K. E., CHAGNE, D., LANDI, M., BOWMAN, J. L. & DAVIES, K. M. 2022. Stress,
1152 senescence, and specialized metabolites in bryophytes. *J Exp Bot,* 73**,** 4396-4411.
1153 LEE, W. S., FU, S. F., LI, Z., MURPHY, A. M., DOBSON, E. A., GARLAND, L., CHALUVADI, S. R., LEWSEY,
1154 M. G., NELSON, R. S. & CARR, J. P. 2016. Salicylic acid treatment and expression of an
1155 RNA-dependent RNA polymerase 1 transgene inhibit lethal symptoms and meristem
1156 invasion during tobacco mosaic virus infection in Nicotiana benthamiana. *BMC Plant*
1157 *Biol,* 16**,** 15.
1158 LEEK, J. T., JOHNSON, W. E., PARKER, H. S., FERTIG, E. J., JAFFE, A.E., ZHANG, Y., STOREY, J. D. &
1159 TORRES, L. C. 2023. sva: Surrogate Variable Analysis.
1160 LETUNIC, I. & BORK, P. 2021. Interactive Tree Of Life (iTOL) v5: an online tool for phylogenetic
1161 tree display and annotation. *Nucleic Acids Research,* 49**,** W293-W296.
1162 LEWSEY, M. G. & CARR, J. P. 2009. Effects of DICER-like proteins 2, 3 and 4 on cucumber mosaic
1163 virus and tobacco mosaic virus infections in salicylic acid-treated plants. *J Gen Virol,* 90**,**
1164 3010-3014.
1165 LI, D., LIU, C. M., LUO, R., SADAKANE, K. & LAM, T. W. 2015. MEGAHIT: an ultra-fast single-node
1166 solution for large and complex metagenomics assembly via succinct de Bruijn graph.
1167 *Bioinformatics,* 31**,** 1674-6.
1168 LIANG, Y., HEYMAN, J., XIANG, Y., VANDENDRIESSCHE, W., CANHER, B., GOEMINNE, G. & DE
1169 VEYLDER, L. 2022. The wound-activated ERF15 transcription factor drives Marchantia
1170 polymorpha regeneration by activating an oxylipin biosynthesis feedback loop. *Sci Adv,*
1171 8**,** eabo7737.
1172 LIM, P. O. & NAM, H. G. 2005. The molecular and genetic control of leaf senescence and longevity
1173 in Arabidopsis. *Curr Top Dev Biol,* 67**,** 49-83.
1174 LIU, C. & NELSON, R. S. 2013. The cell biology of Tobacco mosaic virus replication and movement.
1175 *Front Plant Sci,* 4**,** 12.
1176 LIU, Y., GAO, Q., WU, B., AI, T. & GUO, X. 2009. NgRDR1, an RNA-dependent RNA polymerase
1177 isolated from Nicotiana glutinosa, was involved in biotic and abiotic stresses. *Plant*
1178 *Physiol Biochem,* 47**,** 359-68.
1179 LOPEZ-GOMOLLON, S. & BAULCOMBE, D. C. 2022. Roles of RNA silencing in viral and non-viral
1180 plant immunity and in the crosstalk between disease resistance systems. *Nat Rev Mol*
1181 *Cell Biol,* 23**,** 645-662.
1182 LOVE, M. I., HUBER, W. & ANDERS, S. 2014. Moderated estimation of fold change and dispersion
1183 for RNA-seq data with DESeq2. *Genome Biol,* 15**,** 550.
1184 LUCAS, W. J., GROOVER, A., LICHTENBERGER, R., FURUTA, K., YADAV, S. R., HELARIUTTA, Y., HE, X.
1185 Q., FUKUDA, H., KANG, J., BRADY, S. M., PATRICK, J. W., SPERRY, J., YOSHIDA, A., LOPEZ-
1186 MILLAN, A. F., GRUSAK, M. A. & KACHROO, P. 2013. The plant vascular system: evolution,
1187 development and functions. *J Integr Plant Biol,* 55**,** 294-388.

1188 MANDADI, K. K. & SCHOLTHOF, K. B. 2013. Plant immune responses against viruses: how does a
1189 virus cause disease? *Plant Cell,* 25**,** 1489-505.
1190 MATSUI, H., IWAKAWA, H., HYON, G. S., YOTSUI, I., KATOU, S., MONTE, I., NISHIHAMA, R.,
1191 FRANZEN, R., SOLANO, R. & NAKAGAMI, H. 2020. Isolation of Natural Fungal Pathogens
1192 from Marchantia polymorpha Reveals Antagonism between Salicylic Acid and Jasmonate
1193 during Liverwort-Fungus Interactions. *Plant Cell Physiol,* 61**,** 265-275.
1194 MIFSUD, J. C. O., GALLAGHER, R. V., HOLMES, E. C. & GEOGHEGAN, J. L. 2022. Transcriptome
1195 Mining Expands Knowledge of RNA Viruses across the Plant Kingdom. *J Virol,* 96**,**
1196 e0026022.
1197 MOLDER, F., JABLONSKI, K. P., LETCHER, B., HALL, M. B., TOMKINS-TINCH, C. H., SOCHAT, V.,
1198 FORSTER, J., LEE, S., TWARDZIOK, S. O., KANITZ, A., WILM, A., HOLTGREWE, M.,
1199 RAHMANN, S., NAHNSEN, S. & KOSTER, J. 2021. Sustainable data analysis with
1200 Snakemake. *F1000Res,* 10**,** 33.
1201 MONTE, I., FRANCO-ZORRILLA, J. M., GARCIA-CASADO, G., ZAMARRENO, A. M., GARCIA-MINA, J.
1202 M., NISHIHAMA, R., KOHCHI, T. & SOLANO, R. 2019. A Single JAZ Repressor Controls the
1203 Jasmonate Pathway in Marchantia polymorpha. *Mol Plant,* 12**,** 185-198.
1204 MONTE, I., ISHIDA, S., ZAMARRENO, A. M., HAMBERG, M., FRANCO-ZORRILLA, J. M., GARCIA-
1205 CASADO, G., GOUHIER-DARIMONT, C., REYMOND, P., TAKAHASHI, K., GARCIA-MINA, J.
1206 M., NISHIHAMA, R., KOHCHI, T. & SOLANO, R. 2018. Ligand-receptor co-evolution shaped
1207 the jasmonate pathway in land plants. *Nat Chem Biol,* 14**,** 480-488.
1208 MUSHEGIAN, A., SHIPUNOV, A. & ELENA, S. F. 2016. Changes in the composition of the RNA
1209 virome mark evolutionary transitions in green plants. *BMC Biol,* 14**,** 68.
1210 NERI, U., WOLF, Y. I., ROUX, S., CAMARGO, A. P., LEE, B., KAZLAUSKAS, D., CHEN, I. M., IVANOVA,
1211 N., ZEIGLER ALLEN, L., PAEZ-ESPINO, D., BRYANT, D. A., BHAYA, D., CONSORTIUM, R. N. A.
1212 V. D., KRUPOVIC, M., DOLJA, V. V., KYRPIDES, N. C., KOONIN, E. V. & GOPHNA, U. 2022.
1213 Expansion of the global RNA virome reveals diverse clades of bacteriophages. *Cell,* 185**,**
1214 4023-4037 e18.
1215 NGUYEN, L. T., SCHMIDT, H. A., VON HAESELER, A. & MINH, B. Q. 2015. IQ-TREE: A Fast and
1216 Effective Stochastic Algorithm for Estimating Maximum-Likelihood Phylogenies.
1217 *Molecular Biology and Evolution,* 32**,** 268-274.
1218 NIEHL, A., WYRSCH, I., BOLLER, T. & HEINLEIN, M. 2016. Double-stranded RNAs induce a pattern-
1219 triggered immune signaling pathway in plants. *New Phytol,* 211**,** 1008-19.
1220 PAGAN, I., ALONSO-BLANCO, C. & GARCIA-ARENAL, F. 2008. Host responses in life-history traits
1221 and tolerance to virus infection in Arabidopsis thaliana. *PLoS Pathog,* 4**,** e1000124.
1222 PATRO, R., DUGGAL, G., LOVE, M. I., IRIZARRY, R. A. & KINGSFORD, C. 2017. Salmon provides fast
1223 and bias-aware quantification of transcript expression. *Nature Methods,* 14**,** 417-+.
1224 PEART, J. R., COOK, G., FEYS, B. J., PARKER, J. E. & BAULCOMBE, D. C. 2002. An EDS1 orthologue
1225 is required for N-mediated resistance against tobacco mosaic virus. *Plant J,* 29**,** 569-79.
1226 PRUITT, R. N., LOCCI, F., WANKE, F., ZHANG, L., SAILE, S. C., JOE, A., KARELINA, D., HUA, C.,
1227 FROHLICH, K., WAN, W. L., HU, M., RAO, S., STOLZE, S. C., HARZEN, A., GUST, A. A.,
1228 HARTER, K., JOOSTEN, M., THOMMA, B., ZHOU, J. M., DANGL, J. L., WEIGEL, D.,
1229 NAKAGAMI, H., OECKING, C., KASMI, F. E., PARKER, J. E. & NURNBERGER, T. 2021. The
1230 EDS1-PAD4-ADR1 node mediates Arabidopsis pattern-triggered immunity. *Nature,* 598**,**
1231 495-499.
1232 QUILLIAM, R. S., SWARBRICK, P. J., SCHOLES, J. D. & ROLFE, S. A. 2006. Imaging photosynthesis in
1233 wounded leaves of Arabidopsis thaliana. *J Exp Bot,* 57**,** 55-69.
1234 R.C., S. 1978. Effect of Potato Virus Y and Tobacco Mosaic Virus on Field-Grown Burley Tobacco.
1235 *PHYTOPATHOLOGY,* 68**,** 823-825.

1236 RAKHSHANDEHROO, F., REZAEE, S. & PALUKAITIS, P. 2017. Silencing the tobacco gene for RNA-
1237 dependent RNA polymerase 1 and infection by potato virus Y cause remodeling of
1238 cellular organelles. *Virology,* 510**,** 127-136.
1239 REDKAR, A., GIMENEZ IBANEZ, S., SABALE, M., ZECHMANN, B., SOLANO, R. & DI PIETRO, A. 2022.
1240 Marchantia polymorpha model reveals conserved infection mechanisms in the vascular
1241 wilt fungal pathogen Fusarium oxysporum. *New Phytol,* 234**,** 227-241.
1242 SCHINDELIN, J., ARGANDA-CARRERAS, I., FRISE, E., KAYNIG, V., LONGAIR, M., PIETZSCH, T.,
1243 PREIBISCH, S., RUEDEN, C., SAALFELD, S., SCHMID, B., TINEVEZ, J. Y., WHITE, D. J.,
1244 HARTENSTEIN, V., ELICEIRI, K., TOMANCAK, P. & CARDONA, A. 2012. Fiji: an open-source
1245 platform for biological-image analysis. *Nat Methods,* 9**,** 676-82.
1246 SCHOLTHOF, K. B. 2004. Tobacco mosaic virus: a model system for plant biology. *Annu Rev*
1247 *Phytopathol,* 42**,** 13-34.
1248 SCHOMMER, C., PALATNIK, J. F., AGGARWAL, P., CHETELAT, A., CUBAS, P., FARMER, E. E., NATH,
1249 U. & WEIGEL, D. 2008. Control of jasmonate biosynthesis and senescence by miR319
1250 targets. *PLoS Biol,* 6**,** e230.
1251 SCHWACH, F., VAISTIJ, F. E., JONES, L. & BAULCOMBE, D. C. 2005. An RNA-dependent RNA
1252 polymerase prevents meristem invasion by potato virus X and is required for the activity
1253 but not the production of a systemic silencing signal. *Plant Physiol,* 138**,** 1842-52.
1254 SHENG, Y., YANG, L., LI, C., WANG, Y. & GUO, H. 2019. Transcriptomic changes in Nicotiana
1255 tabacum leaves during mosaic virus infection. *3 Biotech,* 9**,** 220.
1256 SILVESTRI, A., BANSAL, C., & RUBIO-SOMOZA, I. 2024. After silencing suppression: miRNA targets
1257 strike back. Trends in Plant Science. doi.org/10.1016/j.tplants.2024.05.001.
1258 SONESON, C., LOVE, M. I. & ROBINSON, M. D. 2015. Differential analyses for RNA-seq: transcript-
1259 level estimates improve gene-level inferences. *F1000Res,* 4**,** 1521.
1260 VASSEUR, F., BALDRICH, P., JIMENEZ-GONGORA, T., VILLAR-MARTIN, L., WEIGEL, D. & RUBIO-
1261 SOMOZA, I. 2022. miRNA472 deficiency enhances Arabidopsis thaliana defence without
1262 reducing seed production. *bioRxiv,* doi.org/10.1101/2022.12.13.520224
1263 VENDRELL-MIR, P., PERROUD, P. F., HAAS, F. B., MEYBERG, R., CHARLOT, F., RENSING, S. A.,
1264 NOGUE, F. & CASACUBERTA, J. M. 2021. A vertically transmitted amalgavirus is present
1265 in certain accessions of the bryophyte Physcomitrium patens. *Plant J,* 108**,** 1786-1797.
1266 WANG, L., WAN, M. C., LIAO, R. Y., XU, J., XU, Z. G., XUE, H. C., MAI, Y. X. & WANG, J. W. 2023. The
1267 maturation and aging trajectory of Marchantia polymorpha at single-cell resolution. *Dev*
1268 *Cell,* 58**,** 1429-1444 e6.
1269 WANG, X., GOREGAOKER, S. P. & CULVER, J. N. 2009. Interaction of the Tobacco mosaic virus
1270 replicase protein with a NAC domain transcription factor is associated with the
1271 suppression of systemic host defenses. *J Virol,* 83**,** 9720-30.
1272 WHITHAM, S., DINESH-KUMAR, S. P., CHOI, D., HEHL, R., CORR, C. & BAKER, B. 1994. The product
1273 of the tobacco mosaic virus resistance gene N: similarity to toll and the interleukin-1
1274 receptor. *Cell,* 78**,** 1101-15.
1275 XU, T., ZHANG, L., ZHEN, J., FAN, Y., ZHANG, C. & WANG, L. 2013. Expressional and regulatory
1276 characterization of Arabidopsis RNA-dependent RNA polymerase 1. *Planta,* 237**,** 1561-9.
1277 XU, X. J., GENG, C., JIANG, S. Y., ZHU, Q., YAN, Z. Y., TIAN, Y. P. & LI, X. D. 2022. A maize
1278 triacylglycerol lipase inhibits sugarcane mosaic virus infection. *Plant Physiol,* 189**,** 754-
1279 771.
1280 YAMANAKA, T., OHTA, T., TAKAHASHI, M., MESHI, T., SCHMIDT, R., DEAN, C., NAITO, S. &
1281 ISHIKAWA, M. 2000. TOM1, an Arabidopsis gene required for efficient multiplication of
1282 a tobamovirus, encodes a putative transmembrane protein. *Proc Natl Acad Sci U S A,* 97**,**
1283 10107-12.

1284 YING, X., BERA, S., LUI, J., TOSCANO-MORALES, R., JANG, C., YANG, S., HO, J. & SIMON, A.E. 2024.
1285 Umbravirus-like RNA viruses are capable of independent systemic plant infection in the
1286 absence of encoded movement proteins. *PLoS Biol*.
1287 doi.org/10.1371/journal.pbio.3002600.
1288 YING, X. B., DONG, L., ZHU, H., DUAN, C. G., DU, Q. S., LV, D. Q., FANG, Y. Y., GARCIA, J. A., FANG,
1289 R. X. & GUO, H. S. 2010. RNA-dependent RNA polymerase 1 from Nicotiana tabacum
1290 suppresses RNA silencing and enhances viral infection in Nicotiana benthamiana. *Plant*
1291 *Cell,* 22**,** 1358-72.
1292 YOTSUI, I., MATSUI, H., MIYAUCHI, S., IWAKAWA, H., MELKONIAN, K., SCHLUTER, T., MICHAVILA,
1293 S., KANAZAWA, T., NOMURA, Y., STOLZE, S. C., JEON, H. W., YAN, Y., HARZEN, A., SUGANO,
1294 S. S., SHIRAKAWA, M., NISHIHAMA, R., ICHIHASHI, Y., IBANEZ, S. G., SHIRASU, K., UEDA,
1295 T., KOHCHI, T. & NAKAGAMI, H. 2023. LysM-mediated signaling in Marchantia
1296 polymorpha highlights the conservation of pattern-triggered immunity in land plants.
1297 *Curr Biol,* 33**,** 3732-3746 e8.
1298 YU, D., FAN, B., MACFARLANE, S. A. & CHEN, Z. 2003. Analysis of the involvement of an inducible
1299 Arabidopsis RNA-dependent RNA polymerase in antiviral defense. *Mol Plant Microbe*
1300 *Interact,* 16**,** 206-16.
1301 YU, X., XU, Y. & YAN, S. 2021. Salicylic acid and ethylene coordinately promote leaf senescence. *J*
1302 *Integr Plant Biol,* 63**,** 823-827.
1303 ZAMFIR, A. D., BABALOLA, B. M., FRAILE, A., MCLEISH, M. J. & GARCIA-ARENAL, F. 2023.
1304 Tobamoviruses Show Broad Host Ranges and Little Genetic Diversity Among Four Habitat
1305 Types of a Heterogeneous Ecosystem. *Phytopathology,* 113**,** 1697-1707.
1306 ZEINSMASTER D.D & CAROTHERS Z.B 1974. The Fine Structure of Oogenesis in Marchantia
1307 polymorpha. *American Journal of Botany,* 61**,** 499-512.
1308 ZHU, F., XI, D. H., YUAN, S., XU, F., ZHANG, D. W. & LIN, H. H. 2014. Salicylic acid and jasmonic
1309 acid are essential for systemic resistance against tobacco mosaic virus in Nicotiana
1310 benthamiana. *Mol Plant Microbe Interact,* 27**,** 567-77.

1311

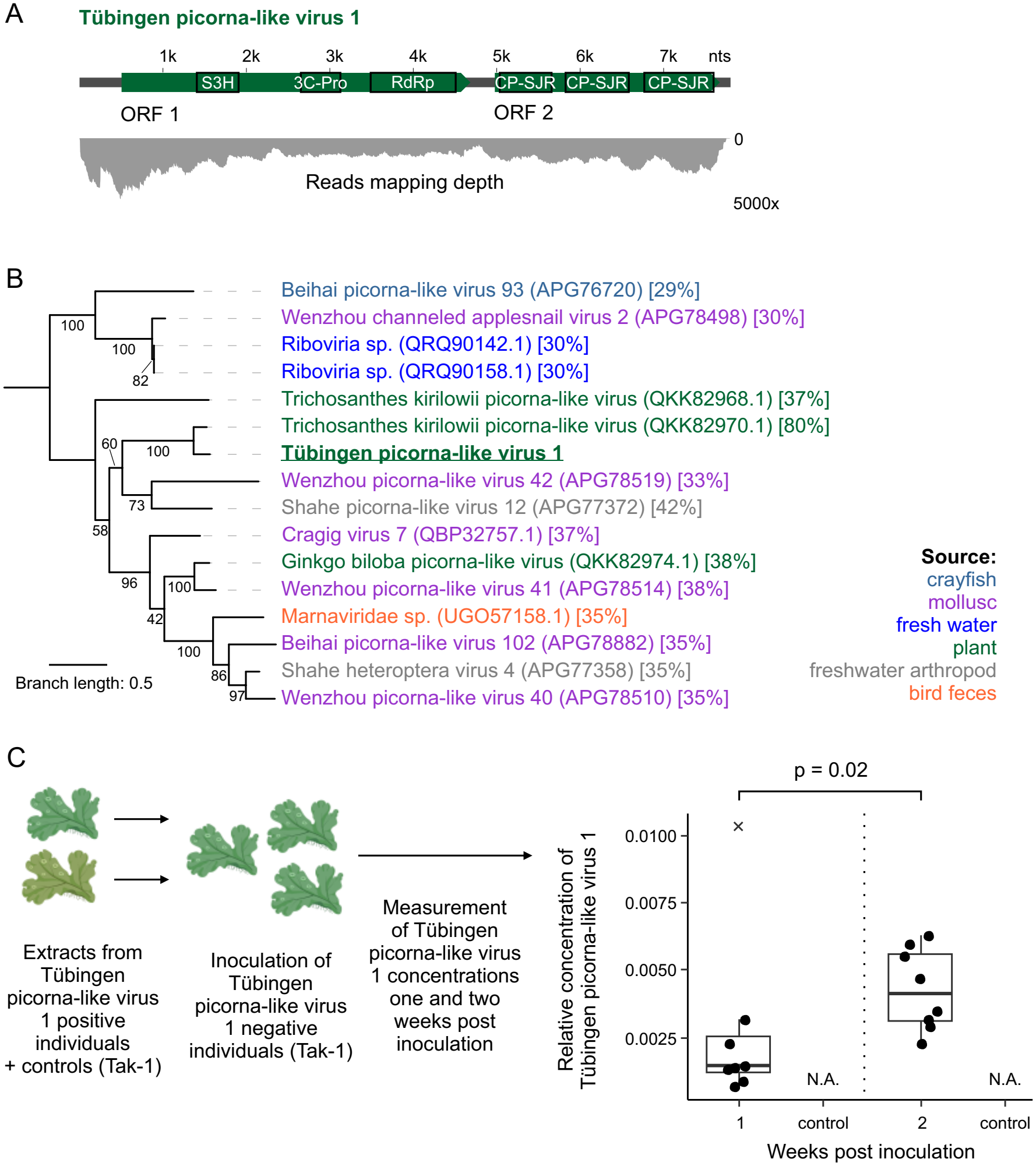
A
Tübingen picorna-like virus 1
1k
2k
3k
4k
5k
6k
7k
nts
S3H
3C-Pro
RdRp
CP-SJR
CP-SJR
CP-SJR
ORF 1
ORF 2
0
Reads mapping depth
5000x
B
Beihai picorna-like virus 93 (APG76720) [29%]
Wenzhou channeled applesnail virus 2 (APG78498) [30%]
Riboviria sp. (QRQ90142.1) [30%]
Riboviria sp. (QRQ90158.1) [30%]
Trichosanthes kirilowii picorna-like virus (QKK82968.1) [37%]
Trichosanthes kirilowii picorna-like virus (QKK82970.1) [80%]
Tübingen picorna-like virus 1
Wenzhou picorna-like virus 42 (APG78519) [33%]
Shahe picorna-like virus 12 (APG77372) [42%]
Cragig virus 7 (QBP32757.1) [37%]
Ginkgo biloba picorna-like virus (QKK82974.1) [38%]
Wenzhou picorna-like virus 41 (APG78514) [38%]
Marnaviridae sp. (UGO57158.1) [35%]
Beihai picorna-like virus 102 (APG78882) [35%]
Shahe heteroptera virus 4 (APG77358) [35%]
Wenzhou picorna-like virus 40 (APG78510) [35%]
100
100
82
60
100
73
58
96
100
42
100
86
97
Branch length: 0.5
Source:
crayfish
mollusc
fresh water
plant
freshwater arthropod
bird feces
C
Extracts from Tübingen picorna-like virus 1 positive individuals + controls (Tak-1)
Inoculation of Tübingen picorna-like virus 1 negative individuals (Tak-1)
Measurement of Tübingen picorna-like virus 1 concentrations one and two weeks post inoculation
p = 0.02
Relative concentration of Tübingen picorna-like virus 1
0.0100
0.0075
0.0050
0.0025
N.A.
N.A.
1
control
2
control
Weeks post inoculation

A

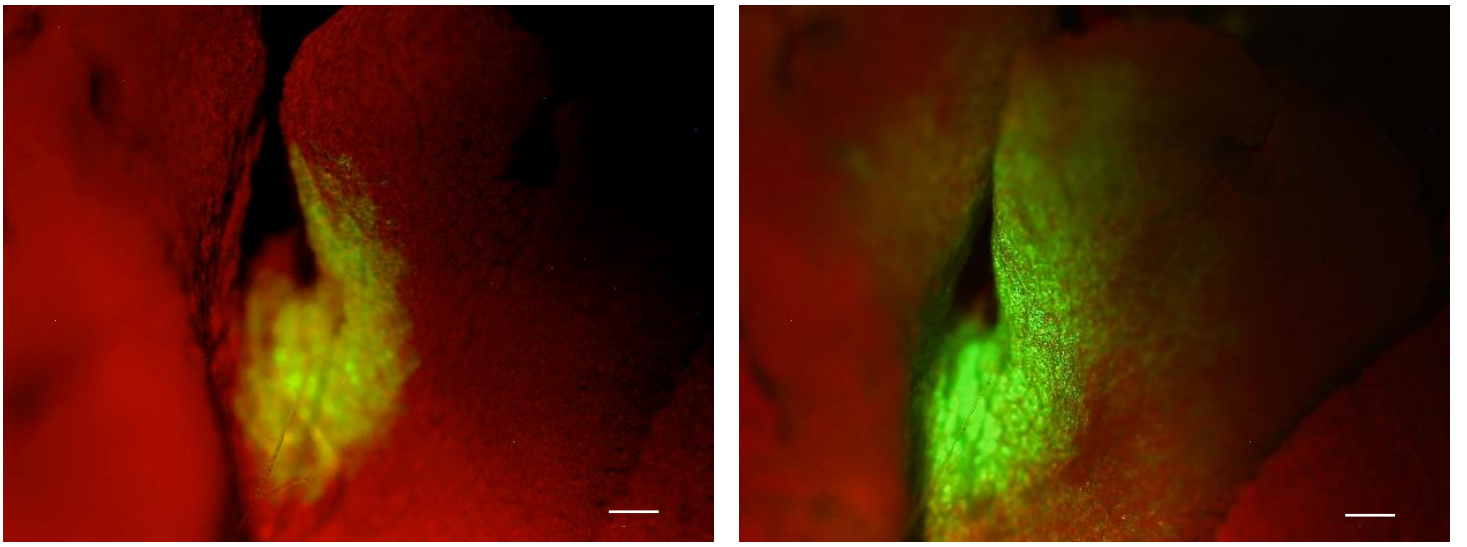

B

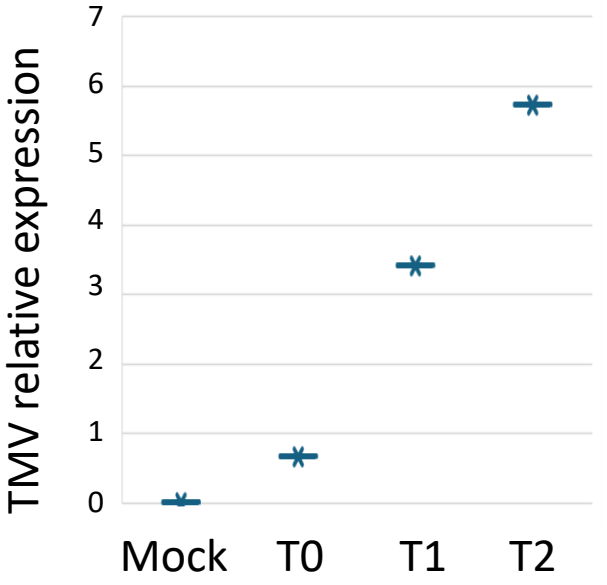

C

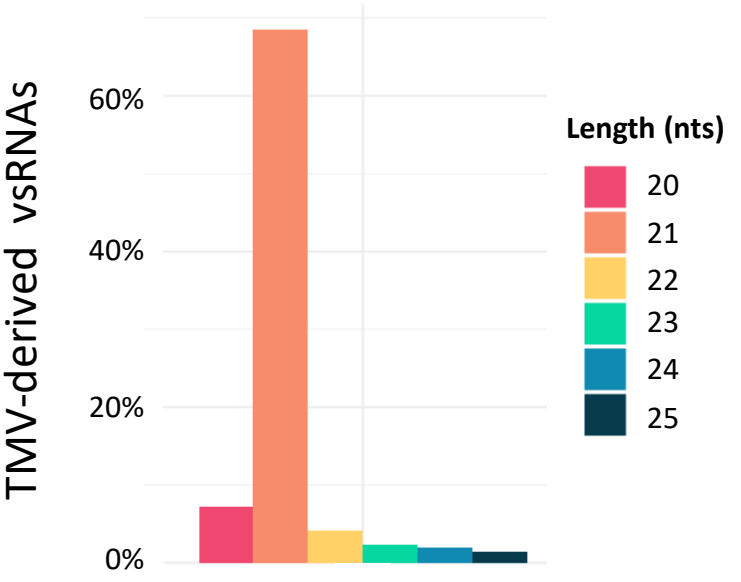

D

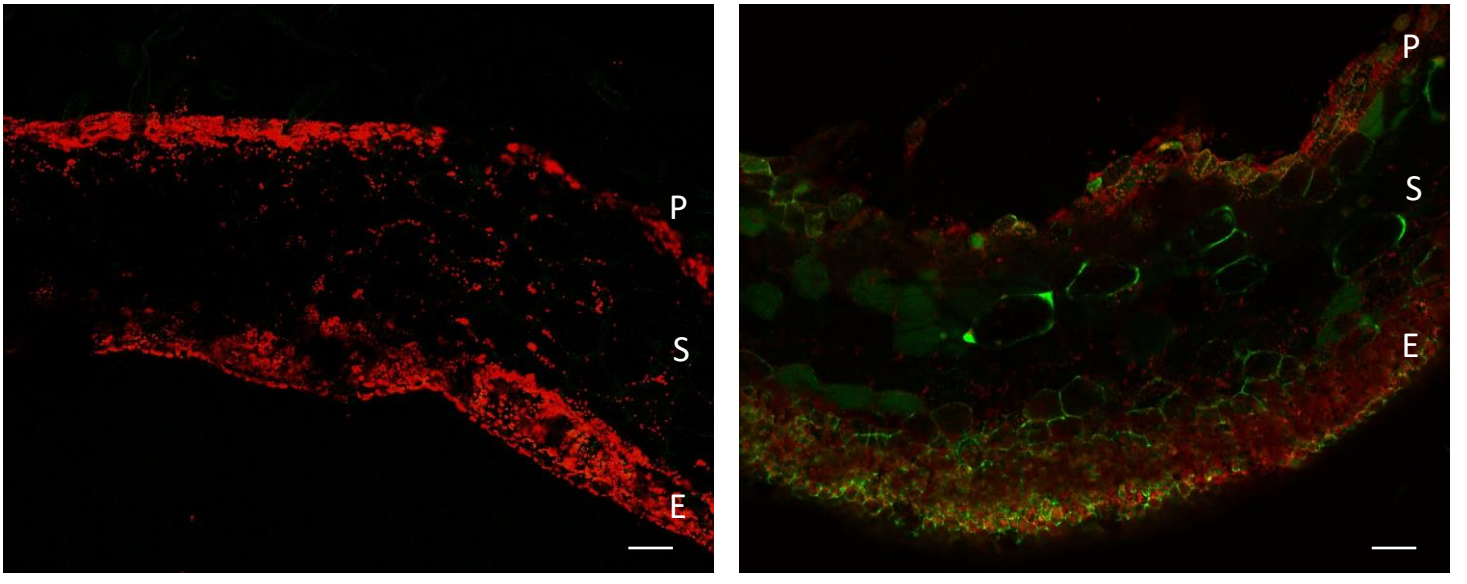

Mock TMV-GFP

A ***PTI Marker genes***

Name	ID	Relative expression level	padj
MpPR9	Mp5g21510	4.04	1.18E-21
MpSYP13B	Mp2g21910	2.34	0.00089
MpCML42	Mp6g18000	1.79	3.01E-17
MpWRKY22	Mp7g17200	1.74	1.82E-32
MpACRE132	Mp1g27170	1.22	1.30E-10

B ***Wound and TMV responsive ERFs***

Name	ID	Relative expression level	padj
MpERF1	Mp7g09350	4.24	0.28
MpERF21	Mp5g22160	1.68	5.91E-05
MpERF8	Mp6g18650	1.48	1.33E-41
MpERF18	Mp5g12480	1.14	0.0015
MpERF15	Mp7g09350	1.06	0.028
MpAP2L1	Mp8g11450	-1.62	4.18E-13
MpERF10	Mp7g00860	-2.83	9.05E-11
MpERF17	Mp4g22280	-2.38	0.00058
MpERF12	Mp6g06870	-2.95	0.014
MpERF16	Mp4g22290	-3.11	0.0004
MpERF13	Mp6g08690	-3.25	4.72E-05

C

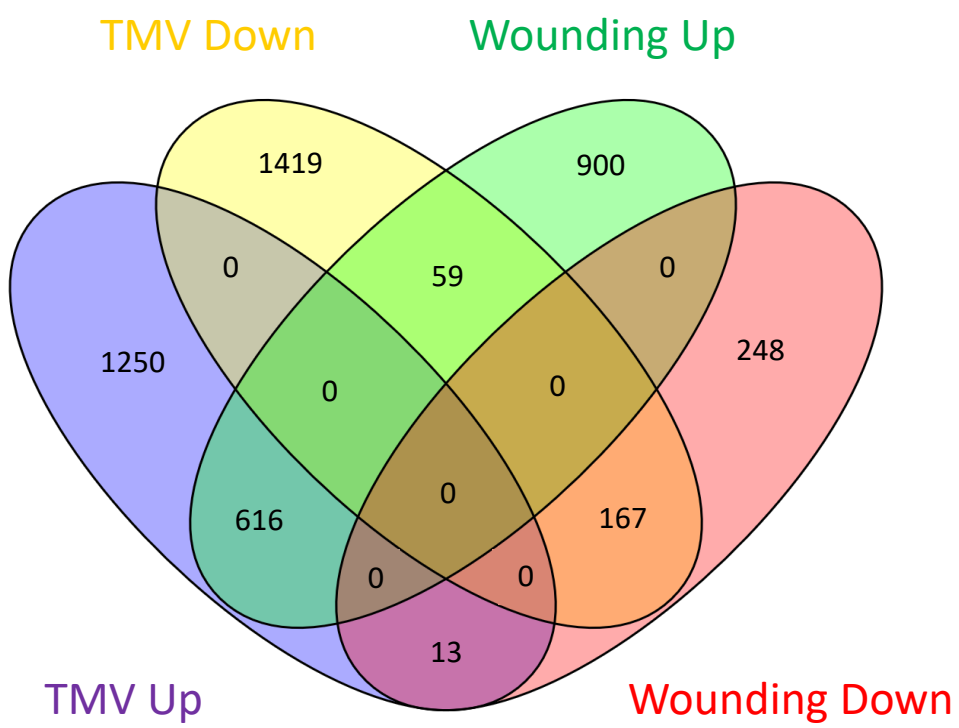

D ***Chitin and TMV responsive WRKYs***

Name	ID	Relative expression level	padj
MpWRKY7	Mp3g17660	3.56	1.68E-34
MpWRKY6	Mp1g08960	2.52	3.71E-17
MpWRKY12	Mp4g00200	1.89	1.90E-11
MpWRKY10	Mp7g06550	1.79	7.31E-06
MpWRKY9	Mp7g17200	1.74	1.82E-32
MpWRKY13	Mp4g00180	1.64	7.72E-11
MpWRKY1	Mp3g00010	1.28	3.79E-25
MpWRKY14	Mp6g16800	1.16	0.013

E ***Infected area***

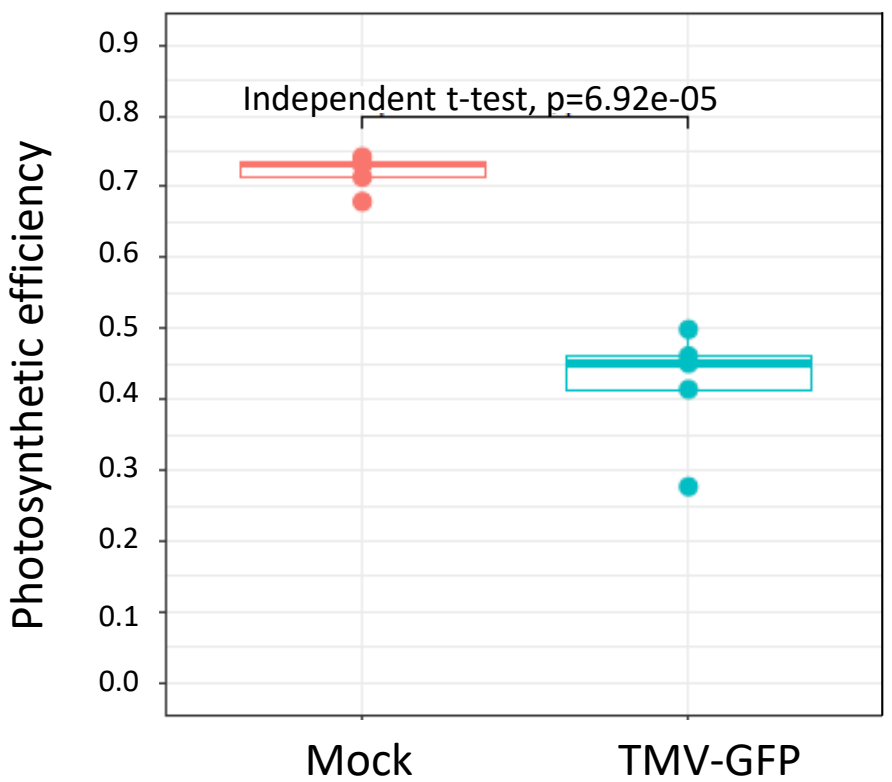

F ***Non-infected area***

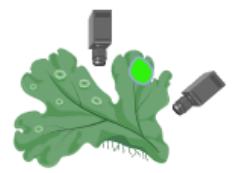

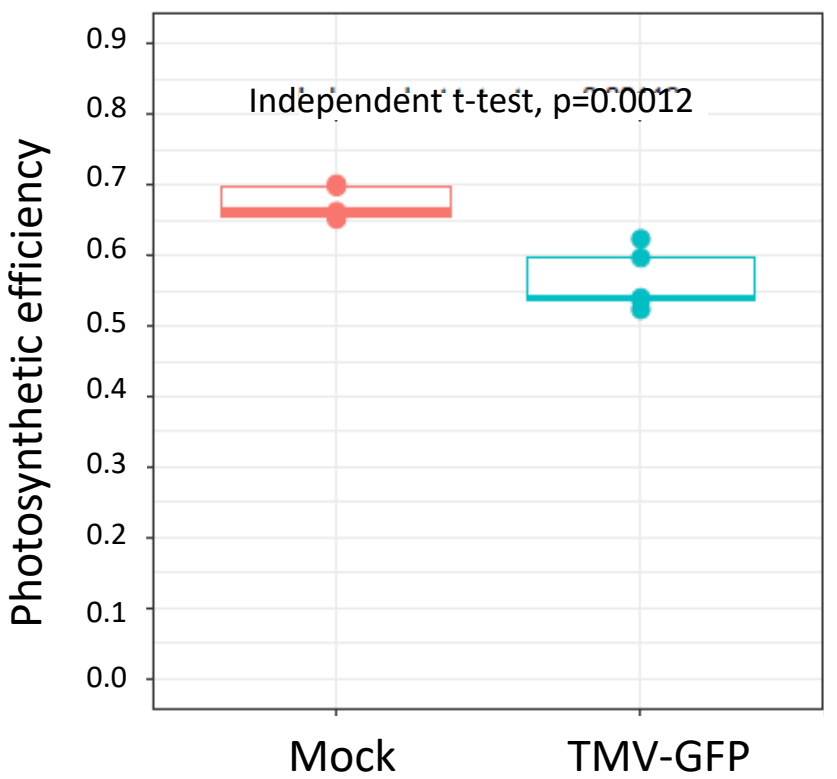

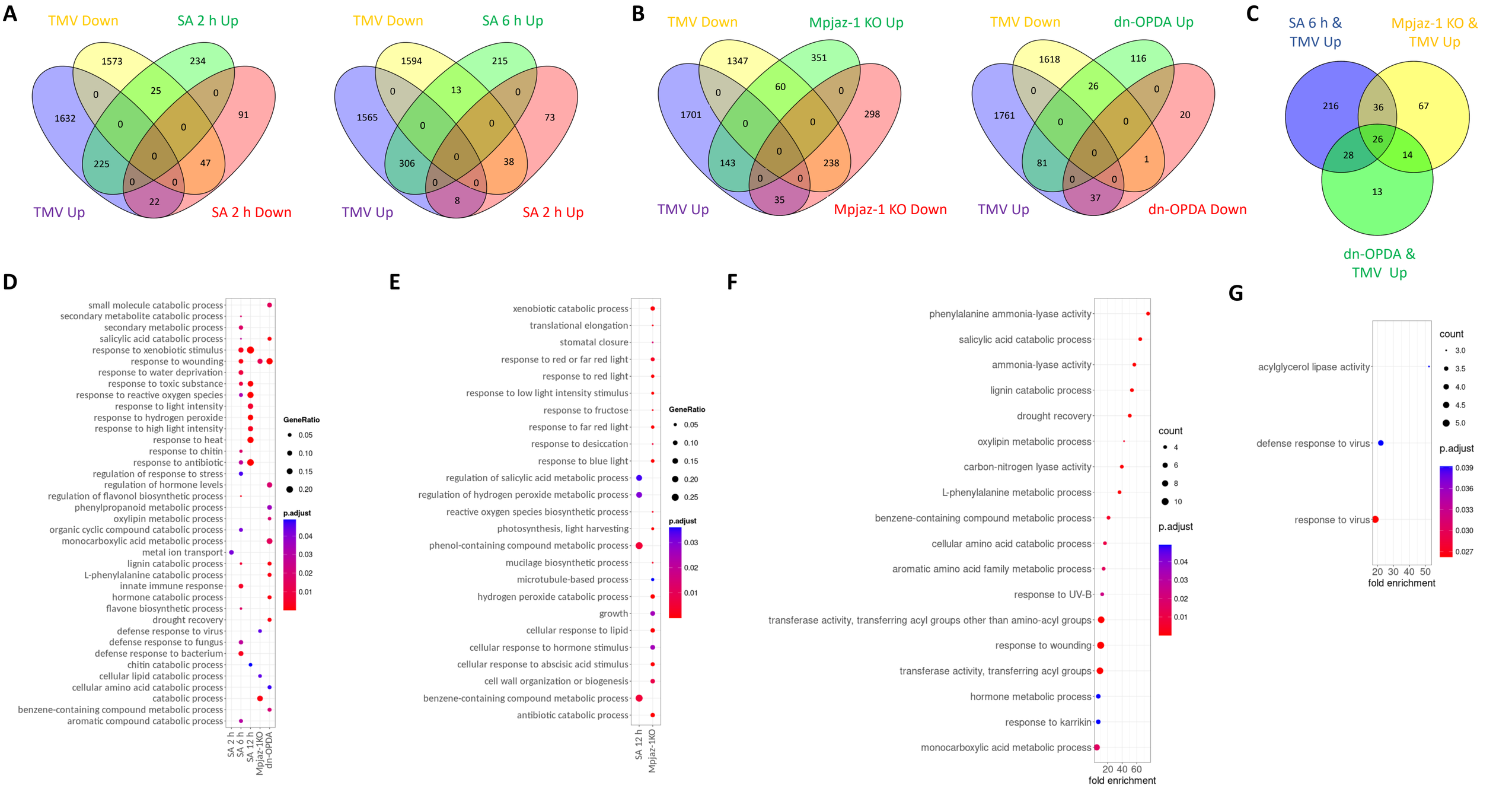
A
TMV Down
SA 2 h Up
1573
234
0
25
0
1632
0
0
91
225
0
47
0
0
22
TMV Up
SA 2 h Down
TMV Down
SA 6 h Up
1594
215
0
13
0
1565
0
0
73
306
0
38
0
0
8
TMV Up
SA 2 h Up
B
TMV Down
Mpjaz-1 KO Up
1347
351
0
60
0
1701
0
0
298
143
0
238
0
0
35
TMV Up
Mpjaz-1 KO Down
TMV Down
dn-OPDA Up
1618
116
0
26
0
1761
0
0
20
81
0
1
0
0
37
TMV Up
dn-OPDA Down
C
SA 6 h &
TMV Up
Mpjaz-1 KO &
TMV Up
216
36
67
26
28
14
13
dn-OPDA &
TMV Up
D
small molecule catabolic process
secondary metabolite catabolic process
secondary metabolic process
salicylic acid catabolic process
response to xenobiotic stimulus
response to wounding
response to water deprivation
response to toxic substance
response to reactive oxygen species
response to light intensity
response to hydrogen peroxide
response to high light intensity
response to heat
response to chitin
response to antibiotic
regulation of response to stress
regulation of hormone levels
regulation of flavonol biosynthetic process
phenylpropanoid metabolic process
oxylipin metabolic process
organic cyclic compound catabolic process
monocarboxylic acid metabolic process
metal ion transport
lignin catabolic process
L-phenylalanine catabolic process
innate immune response
hormone catabolic process
flavone biosynthetic process
drought recovery
defense response to virus
defense response to fungus
defense response to bacterium
chitin catabolic process
cellular lipid catabolic process
cellular amino acid catabolic process
catabolic process
benzene-containing compound metabolic process
aromatic compound catabolic process
SA 2 h
SA 6 h
SA 12 h
Mpjaz-1KO
dn-OPDA
GeneRatio
0.05
0.10
0.15
0.20
p.adjust
0.04
0.03
0.02
0.01
E
xenobiotic catabolic process
translational elongation
stomatal closure
response to red or far red light
response to red light
response to low light intensity stimulus
response to fructose
response to far red light
response to desiccation
response to blue light
regulation of salicylic acid metabolic process
regulation of hydrogen peroxide metabolic process
reactive oxygen species biosynthetic process
photosynthesis, light harvesting
phenol-containing compound metabolic process
mucilage biosynthetic process
microtubule-based process
hydrogen peroxide catabolic process
growth
cellular response to lipid
cellular response to hormone stimulus
cellular response to abscisic acid stimulus
cell wall organization or biogenesis
benzene-containing compound metabolic process
antibiotic catabolic process
SA 12 h
Mpjaz-1KO
GeneRatio
0.05
0.10
0.15
0.20
0.25
p.adjust
0.03
0.02
0.01
F
phenylalanine ammonia-lyase activity
salicylic acid catabolic process
ammonia-lyase activity
lignin catabolic process
drought recovery
oxylipin metabolic process
carbon-nitrogen lyase activity
L-phenylalanine metabolic process
benzene-containing compound metabolic process
cellular amino acid catabolic process
aromatic amino acid family metabolic process
response to UV-B
transferase activity, transferring acyl groups other than amino-acyl groups
response to wounding
transferase activity, transferring acyl groups
hormone metabolic process
response to karrikin
monocarboxylic acid metabolic process
20 40 60
fold enrichment
count
4
6
8
10
p.adjust
0.04
0.03
0.02
0.01
G
acylglycerol lipase activity
defense response to virus
response to virus
20 30 40 50
fold enrichment
count
3.0
3.5
4.0
4.5
5.0
p.adjust
0.039
0.036
0.033
0.030
0.027

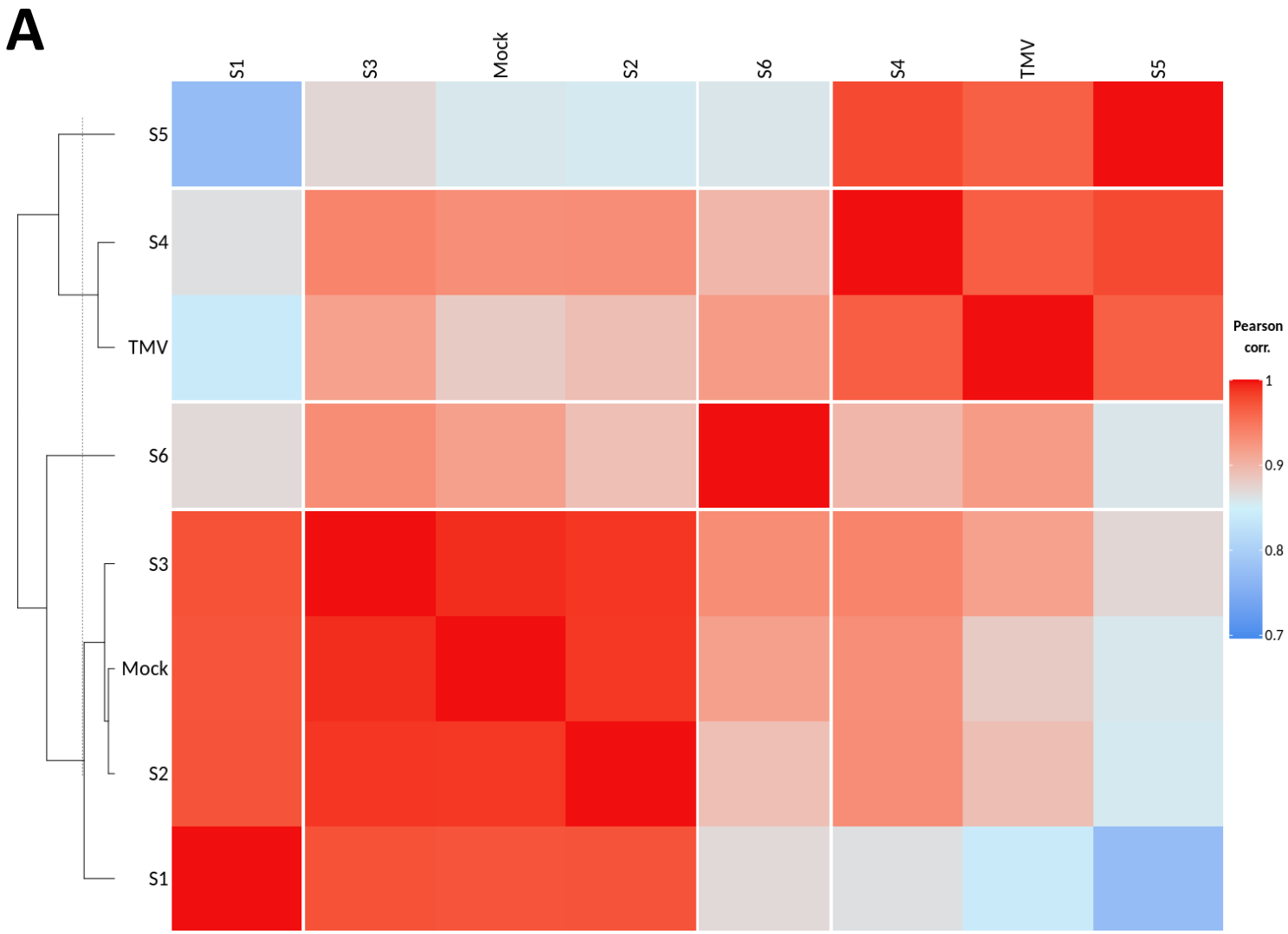
A
S1
S3
Mock
S2
S6
S4
TMV
S5
S5
S4
TMV
S6
S3
Mock
S2
S1
Pearson corr.
1
0.9
0.8
0.7

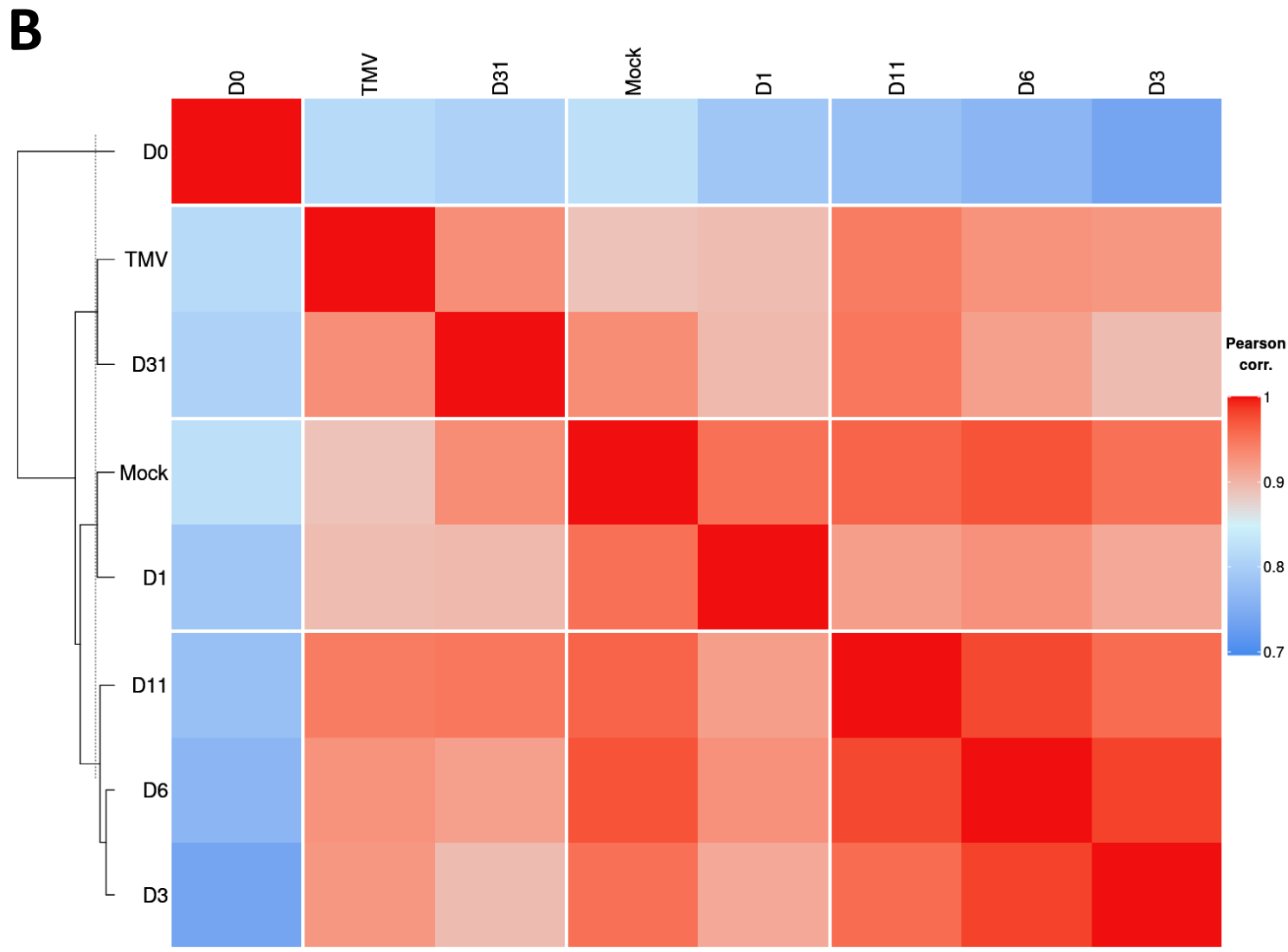
B
D0
TMV
D31
Mock
D1
D11
D6
D3
D0
TMV
D31
Mock
D1
D11
D6
D3
Pearson corr.
1
0.9
0.8
0.7

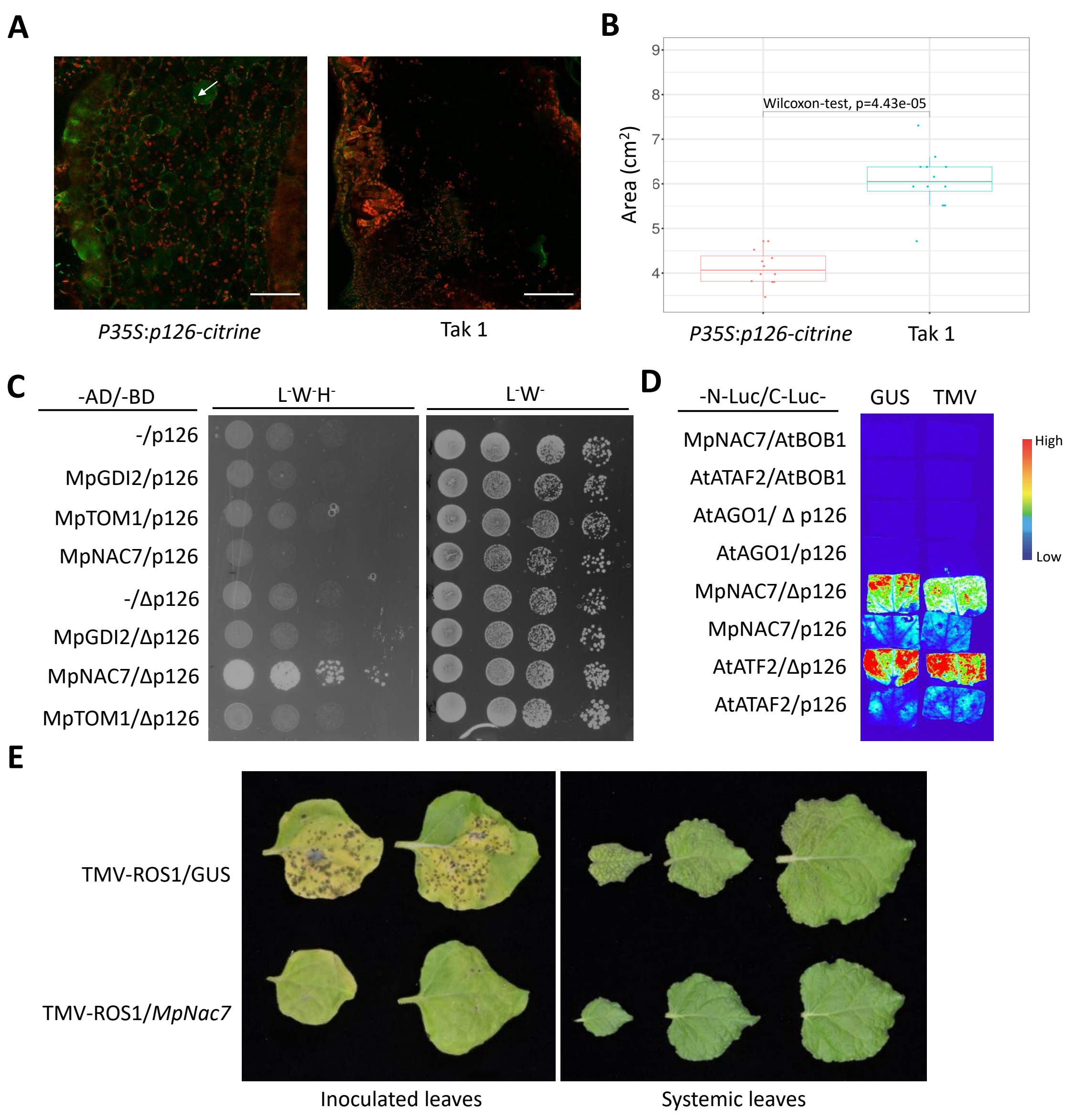
A
P35S:p126-citrine
Tak 1
B
Wilcoxon-test, p=4.43e-05
Area (cm2)
9
8
7
6
5
4
P35S:p126-citrine
Tak 1
C
-AD/-BD
L-W-H-
L-W-
-/p126
MpGDI2/p126
MpTOM1/p126
MpNAC7/p126
-/Δp126
MpGDI2/Δp126
MpNAC7/Δp126
MpTOM1/Δp126
D
-N-Luc/C-Luc-
GUS
TMV
MpNAC7/AtBOB1
AtATAF2/AtBOB1
AtAGO1/ Δ p126
AtAGO1/p126
MpNAC7/Δp126
MpNAC7/p126
AtATF2/Δp126
AtATAF2/p126
High
Low
E
TMV-ROS1/GUS
TMV-ROS1/MpNac7
Inoculated leaves
Systemic leaves